IMPACT OF AD HOC IMPROVEMENT OF DECAY AND CROSS-SECTION DATA ON THE PREDICTION OF FUSION-NEUTRON-INDUCED RADIOACTIVITY IN ZIRCONIUM AND TUNGSTEN

BLANKET ENGINEERING

KEYWORDS: *induced radioactivity, nuclear data, curve fitting*

INSOO JUN, MOHAMED A. ABDOU, and ANIL KUMAR
University of California, Los Angeles, Los Angeles, California 90024

Received September 30, 1992
Accepted for Publication June 16, 1993

Measured decay rates resulting from neutron irradiation of zirconium and tungsten samples in a typical fusion environment have been compared with the computed values, and the sources of errors in the data and the calculational method have been identified. Comparison of four codes showed large differences that arise mainly from differences in the data libraries provided with these codes. The following reactions were found to be most important in terms of their contribution to the decay photon emission rate: $^{90}Zr(n,2n)^{89m+g}Zr$, $^{90}Zr(n,p)^{90m}Y$, $^{90}Zr(n,\alpha)^{87m}Sr$, $^{91}Zr(n,p)^{91m}Y$, $^{186}W(n,\gamma)^{187}W$, $^{186}W(n,p)^{186}Ta$, $^{186}W(n,np)(n,d)^{185}Ta$, $^{184}W(n,p)^{184}Ta$, $^{183}W(n,p)^{183}Ta$, $^{182}W(n,p)^{182}Ta$, *and* $^{186}W(n,\alpha)^{183}Hf$. *However, decay data and cross sections for these reactions are not adequate in currently available libraries. An effort was made to improve the decay data by using the values from the most recent Table of Radioactive Isotopes and to improve the cross sections by using a simple curve-fitting procedure. Modified or improved decay data and cross sections were implemented in a representative code, and the computation was performed again. A great improvement in the computed results was observed for both sample cases. This work can easily be extended to other fusion-relevant materials by utilizing the methodology presented here.*

The improved decay and cross-section data were applied to an International Thermonuclear Experimental Reactor (ITER) blanket using tungsten as a first-wall coating material and Li_2ZrO_3 *as a breeding material. The specific photon yield in each zone was computed, and as much as three orders of magnitude difference in the photon yield in the tungsten zone and ~10 to 15% difference in the zirconium-containing breeding zone were observed between the results using the improved decay and cross-section data and those using the original data.*

I. INTRODUCTION

Fusion-neutron-induced radioactivity is one of the important design issues in fusion reactor studies and has been the subject of extensive research.[1-36] Problems associated with neutron-induced radioactivity in the fusion environment can be categorized broadly into three areas[37]: (a) reactor maintenance, (b) reactor safety and biological hazard, and (c) waste disposal. The selection of materials for reactor components such as first wall, blanket, and shield is influenced by these factors. Therefore, accurate prediction of induced radioactivity is necessary for the development of fusion reactors.

The calculation of radioactivity depends on inputs such as the neutron energy spectrum, transmutation cross sections, decay data, and initial material composition of the fusion system as well as an accurate mathematical method. Many researchers throughout the world have developed computer codes, which consist of a main program and a basic nuclear data library, to calculate the radioactivity in fusion systems. These

codes and data libraries must be verified to establish confidence in their predictive capabilities and to estimate the accuracy of the calculation. Recently, some efforts[38,39] have been made to verify these computer codes in terms of not only the verification of the mathematical models embedded in the computer program, but also the reliability of the basic nuclear data employed. The work by Cheng et al.[38] is a representative example. However, the main problem associated with that work was the lack of experimental results from integral measurements against which calculational results could be compared. This paper is concerned with the verification and improvement of the capability to predict radioactivity, based on experimental data from recent integral measurements. Of the many computer codes developed thus far, four representative codes are selected: REAC*2 (Ref. 40), DKRICF (Ref. 41), and RACC (Ref. 42), from the United States, and ACT4, which is the main activation calculating module in the THIDA-2 code,[43] from Japan.

Recently, extensive studies[44-51] related to this subject have been performed under the U.S. Department of Energy/Japan Atomic Energy Research Institute (DOE/JAERI) collaborative program. Integrated decay gamma emission rates resulting from fusion-neutron irradiation of various materials have been measured and compared with the values computed by using the codes mentioned earlier. It has been reported that the large discrepancies observed for practically all materials, even for integrated rates, are mainly due to inadequate activation cross sections and decay data. In particular, large discrepancies have been shown for nickel, molybdenum, titanium, tungsten, indium, tantalum, cobalt, zirconium, lead, zinc, silver, and tin.

The work presented here uses the results of integral measurements from the DOE/JAERI program and focuses on ways of improving the decay and cross-section data libraries of the codes so as to improve the agreement between the measured and computed values. Even though many materials were irradiated in this program, only results from zirconium and tungsten samples are studied completely in this paper. A complete study of these two materials has direct application to real fusion reactors, where zirconium can be used as the solid breeder material in the form of Li_2ZrO_3 and tungsten can be used as a shielding material and coating for the plasma-facing components. Also, the methodology employed here is applicable to other materials.

Section II briefly describes the experimental configuration where the decay rates are measured. In Sec. III, the different mathematical models used in the codes are tested and discussed. In Sec. IV, the observed discrepancies in the decay and cross-section data from the codes are explained, while Secs. V and VI deal with the improvement of the decay and cross-section data, respectively. In Sec. VII, the effect of the improved decay and cross-section data on the prediction of decay rates is discussed. In Sec. VIII, the corrected and modified data are applied to the activation analysis for the International Thermonuclear Experimental Reactor (ITER) outboard to see the effect of the improved data on the prediction of radioactive inventory in a realistic system. Finally, in Sec. IX, the summary and concluding remarks are presented.

II. EXPERIMENT

The decay photon spectra of radioactive nuclides resulting from simulated fusion-neutron irradiation of various materials were measured under the DOE/JAERI collaborative program.[44-51] The fusion neutrons were generated by impinging an accelerated 350-keV deuterium beam on a tritiated target. The materials irradiated in the experiment included iron, chromium, nickel, molybdenum, Type 316 stainless steel, Mn-Cu alloy, vanadium, titanium, cobalt, aluminum, silicon, zirconium, niobium, tungsten, gold, indium, magnesium, tantalum, $YBa_2Cu_3O_7$, and $ErBa_2Cu_3O_7$. Of these, gold, indium, aluminum, niobium, and iron were also used for monitoring the local neutron energy spectrum.

As shown in Fig. 1, each sample was located at two different positions: (a) at 10 cm from the target at a 30-deg angle to the incident D^+ beam direction to simulate the spectral conditions close to the first wall in fusion reactors and (b) at 5 cm inside the Li_2O zone (82 cm from the target) in an off-center drawer to simulate the softer neutron spectral environment. The neutron energy spectra at the two sample positions were obtained by MCNP calculation[52] and are depicted in Fig. 2. More detailed calculations for the neutron spectrum can be found in Refs. 46 and 47. It is obvious that the dominance of 14-MeV neutrons in the 82-cm spectrum is lower than in the 10-cm spectrum.

Since the amount of decay photons also depends on the irradiation time and the waiting (cooling) time, each sample was subjected to different irradiation and cooling times. For example, two iron samples were located at 10 cm from the target. One sample was removed after 30 min of irradiation, and the decay photons were counted after 22.4 min of waiting time; the other sample was irradiated for 9 h, and the decay photons were measured after waiting times of 3 h, 22.3 min and 5 days, 13.7 h. The same strategy was also applied to the samples located at 5 cm inside the Li_2O zone. In this way, it was possible to see the effects of (a) different neutron energy spectra, (b) different irradiation times, and (c) different cooling times on the decay rates of various radioactive products in a simulated fusion environment. Interested readers are advised to consult Refs. 44 through 51 for more detailed information on these experiments.

The main objective of measuring the decay rates was to provide a basis for verifying the radioactivity codes, especially their nuclear data libraries. The

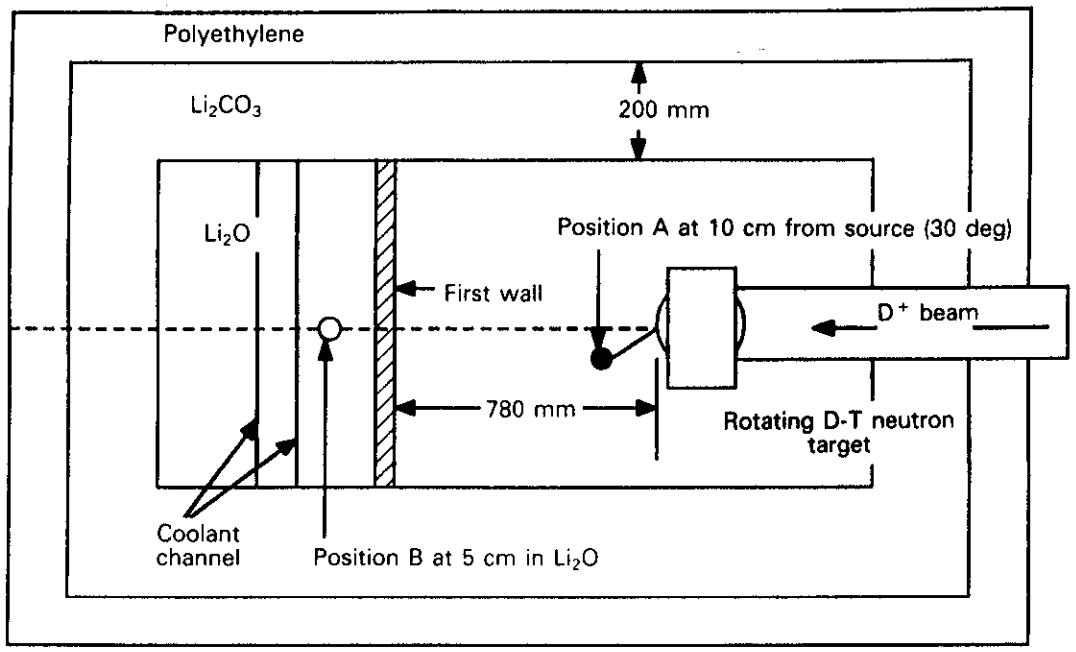

Fig. 1. Experimental setup used in measuring the decay rates from neutron irradiation of various materials.

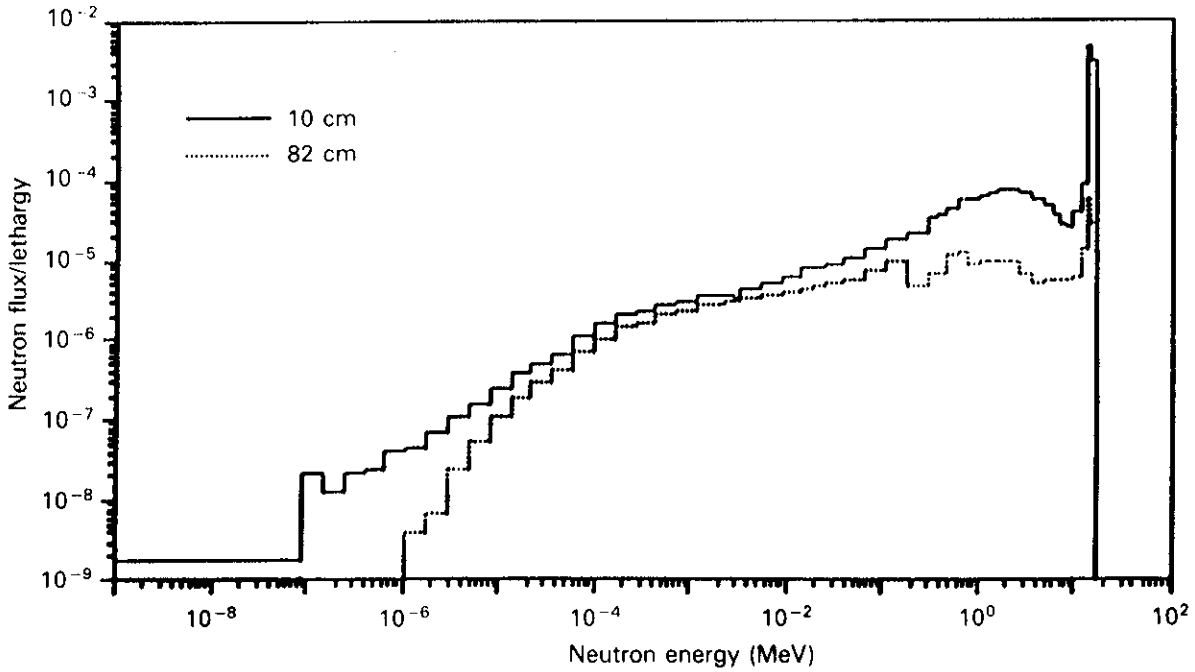

Fig. 2. Neutron spectra obtained by using MCNP Monte Carlo simulation at two different sample positions.

nuclear data include the decay and cross-section data. The decay photon spectra emitted from each sample after the specified irradiation and cooling times are calculated and compared with the experimentally obtained values by using two different neutron spectra.

III. METHOD TEST

Since it is very natural to check the mathematical models used in each code before proceeding to the analysis of the experimental results, a comparison study

TABLE I

Activity (Ci/cm^3) Due to ^{56}Mn Resulting from the ^{56}Fe(n,p) Reaction in Case 1

	Manual	REAC*2	DKRICF	RACC	ACT4
1 h	383.53	383.63	383.7	383.85	383.63
1 yr	1622.66	1622.6	1628	1627.7	1627.7

of the codes was conducted. All the pertinent input data, which include the cross-section data, decay data, irradiation and cooling times, and material compositions, were kept the same for all the codes. Two different cases were considered: (a) a case that is simple enough that a manual calculation is possible without much effort and (b) a more complicated case with more isotopes so as to have a larger number of radioactive products. The explanations and calculational results for both cases are presented in the following.

III.A. Case 1: A Very Simple Problem

A very simple problem was set up to make a hand calculation possible with little difficulty. It was assumed that 100% ^{56}Fe was irradiated by a 14-MeV monoenergetic neutron source with a flux of 10^{14} n/cm^2·s. Only the ^{56}Fe$(n,p)^{56}$Mn reaction was considered, and the corresponding cross section at 14 MeV was taken as 1 b. The decay constant for ^{56}Mn used in all the codes was set to be 7.4660×10^{-5}/s. Then, radioactivity due to ^{56}Mn after 1 h and 1 yr of irradiation were calculated manually as well as by using the four codes. As shown in Table I, the results obtained are in very good agreement with each other. Small differences seem to originate from the rounding-off error in each code.

III.B. Case 2: A More Complex Problem

In this case, a natural iron sample whose isotopic composition is shown in Table II was assumed to be irradiated for 30 min by the 10-cm neutron spectrum described in Sec. II. This spectrum corresponds to $\sim 10^9$ to 10^{10} n/cm^2·s, which is four to five orders of magnitude lower than the flux level in case 1. Thus, in this low-fluence situation, the secondary neutron reactions are insignificant, so that all the code results are due to the primary reactions. However, if one increases the fluence level, the secondary neutron reactions will begin to contribute. Large fluence level increases were not included in this study in order to concentrate only on the results from the primary reactions. The results are normalized to 10^{12} source neutron/s. Activity due to ^{56}Mn, which can originate from the ^{56}Fe(n,p), ^{57}Fe$(n,np/d)$, ^{58}Fe(n,t), and ^{55}Mn(n,γ) reactions, was calculated by the four codes, and the results were compared with each other. However, only the first three reactions were considered in this study. The ENDF/B-VI data[53] were used for the ^{56}Fe(n,p) and ^{57}Fe$(n,np/d)$ reaction cross sections, and the data in DKRICF were used for the ^{58}Fe(n,t) reaction cross section. The necessary decay data were also taken from the DKRICF data library, so that the only major difference between the calculations is the mathematical model used in each code.

TABLE II

Isotopic Composition of Natural Iron Sample Used in Case 2

Element	Natural Isotopes	Natural Abundance (%)	Number Density[a]
$_{26}$Fe (99.92 wt%)	^{54}Fe	5.8	6.2558E+20[b]
	^{56}Fe	91.72	9.8852E+21
	^{57}Fe	2.2	2.3729E+20
	^{58}Fe	0.28	3.0200E+20
$_{25}$Mn (0.059 wt%)	^{55}Mn	100	6.4678E+18
$_{6}$C (0.02 wt%)	^{12}C	98.9	9.918E+18
	^{13}C	1.1	1.103E+17

[a]Number densities were calculated based on a sample density of 1 g/cm^3.
[b]Read as 6.2558×10^{20}.

The results are summarized in Table III. As shown, the result from RACC is ~2% lower than that of DKRICF, whereas the result from REAC*2 is ~3% larger than that of DKRICF. The results of RACC and REAC*2 differ by 5 to 6%. The ACT4 result is very similar to that of DKRICF. The differences in the calculational results among the codes seem to originate from (a) the numerical error during the flux conversion (each code has a different group structure, and the flux

TABLE III

Calculated Activity (Ci/cm^3) of ^{56}Mn for Case 2

DKRICF	RACC	REAC*2	ACT4
3.253E−6[a]	3.17716E−6 (0.977)[b]	3.3650E−6 (1.034)[b]	3.22166E−6 (0.993)[b]

[a]Read as 3.2530×10^{-6}.
[b]Relative to DKRICF.

is converted for each code by using total flux conservation) and (b) the rounding-off error in each code.

Therefore, it can be concluded that if the values calculated by the four codes disagree by a large amount, it is mainly due to the inconsistency of the nuclear data used in each code, not to the mathematical models employed. This is because we are dealing with much larger discrepancies than the ones presented in Table I when we compare the computed results with the experimental data, as can be seen later. However, note that this conclusion applies only to our experimental conditions, where only relatively short irradiation times are concerned. For very long irradiation times, the secondary neutron reactions, such as $^{56}Fe(n,p)^{56}Mn(n,p)^{56}Cr$, become important.

IV. OBSERVED DISCREPANCIES

As stated earlier, the main objective of this study is to verify the ability of the existing codes to predict the radioactivity and its related parameters in a typical fusion environment by comparing calculated values with experimental data. Our main tools for calculating the radioactivity are computer codes, which are governed by different mathematical models and different nuclear data sets. Since it was verified in Sec. III that the mathematical models used in different computer codes are not likely to contribute to large discrepancies, we focus on checking and improving the basic nuclear data employed in each code.

Measured decay photon yields as a function of photon energy resulting from typical fusion-neutron irradiation of zirconium and tungsten samples are displayed in Fig. 3 for zirconium and in Fig. 4 for tungsten. A detailed description of the experimental error can be found in Ref. 47. Three different conditions for zirconium and two for tungsten were considered to see the effect of various irradiation and cooling time combinations and of the neutron energy spectrum. Table IV summarizes these time histories for each sample. Note that the number of photons in each energy peak was actually measured in the experiment and that the number of photons counted for each peak was converted into decay photon yield by the following relation:

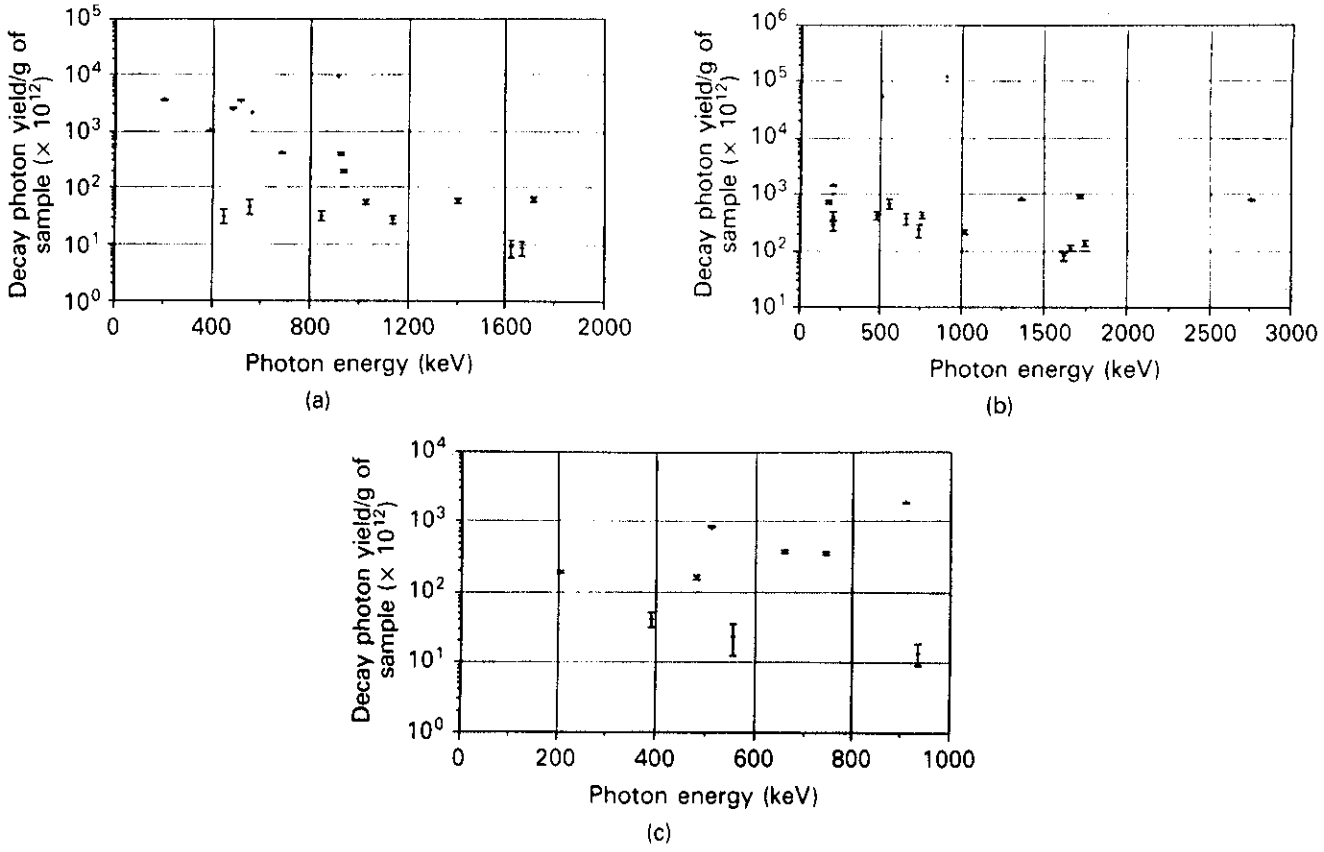

Fig. 3. Decay rates as a function of photon energy resulting from fusion-neutron irradiation to a zirconium sample at 10-cm spectrum for (a) $T_r = 30$ min and $T_c = 56.5$ min and for (b) $T_r = 9$ h and $T_c = 17$ h, 15.7 min; and (c) at 82-cm spectrum for $T_r = 10$ h and $T_c = 3$ h, 13.5 min.

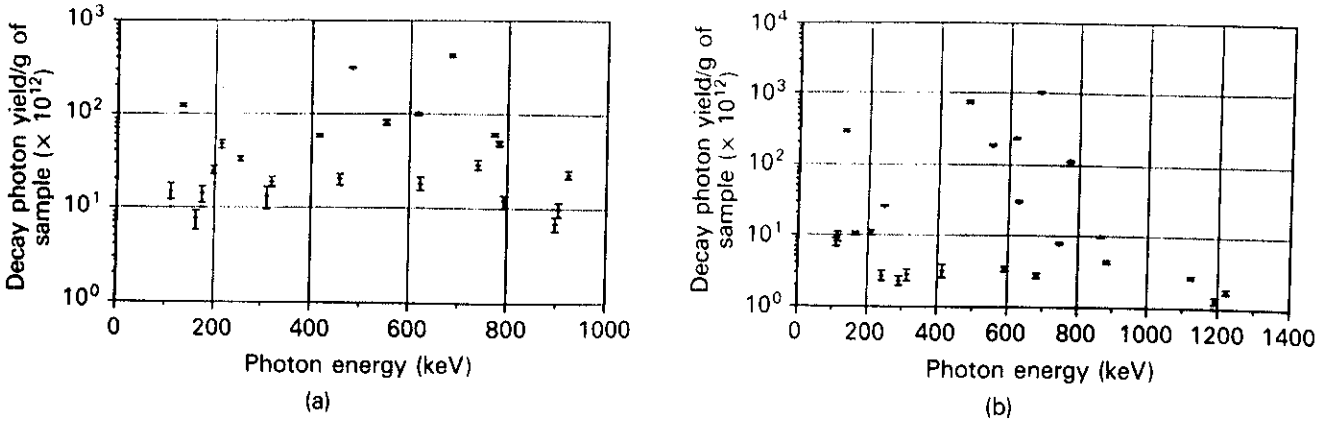

Fig. 4. Decay rates as a function of photon energy resulting from fusion-neutron irradiation to a tungsten sample at 10-cm spectrum for (a) T_r = 30 min and T_c = 37.3 min and for (b) T_r = 9 h and T_c = 2 days, 19 h, 3.5 min.

TABLE IV

Time Specifications for the Zirconium and Tungsten Samples

Material	Distance from Source (cm)	Irradiation Time	Cooling Time	Counting Time
Zirconium	10	30 min	56.5 min	18.9 min
	10	9 h	17 h, 15.7 min	40.0 min
	82	10 h	3 h, 13.5 min	33.7 min
Tungsten	10	30 min	37.3 min	15.5 min
	10	9 h	2 days, 19 h, 3.5 min	18 h, 22.7 min

$$DY\ (\text{number of photons emitted per unit mass of sample}) = \frac{\lambda N_{count}}{W[1-\exp(-\lambda \Delta t_m)]} , \quad (1)$$

where

λ = decay constant

N_{count} = number of photons counted for a particular peak

W = mass of sample

Δt_m = counting time.

Of course, N_{count} should be corrected by various factors, for example, by detector efficiency, background count, attenuation of decay gammas emitted in a sample, and the variation of the source neutron intensity during irradiation. Also, note that the decay photon yields were normalized to per gram of sample per 10^{12} 14-MeV source neutrons per second to make it easy to compare with the calculational results.

After the origins of each measured peak were identified, the peaks that originated from the same radionuclide were summed up. Their total decay photon yields are redrawn in Fig. 5 for zirconium and Fig. 6 for tungsten as functions of the half-lives of the nuclides. Also noted in the figures are their respective fractions of the total decay photon yield. It turns out that for zirconium, ^{89}Zr, ^{89m}Y, ^{91m}Y, and ^{87m}Sr are major contributing nuclides, whereas ^{187}W, ^{186}Ta, ^{184}Ta, and ^{183}Hf are major contributors for tungsten. Calculations by the four codes were carried out, and the computed results were compared with the measured decay photon yields. The results of this comparison are summarized in Figs. 7 and 8 in the form of computed to experimental value (C/E) ratios, again as a function of the half-lives of the radionuclides produced. Note that the DKRICF results are not shown in these figures since DKRICF does not present the contributions of each single nuclide but gives the total decay photons in the form of prescribed energy bins. Hence, only the status of the

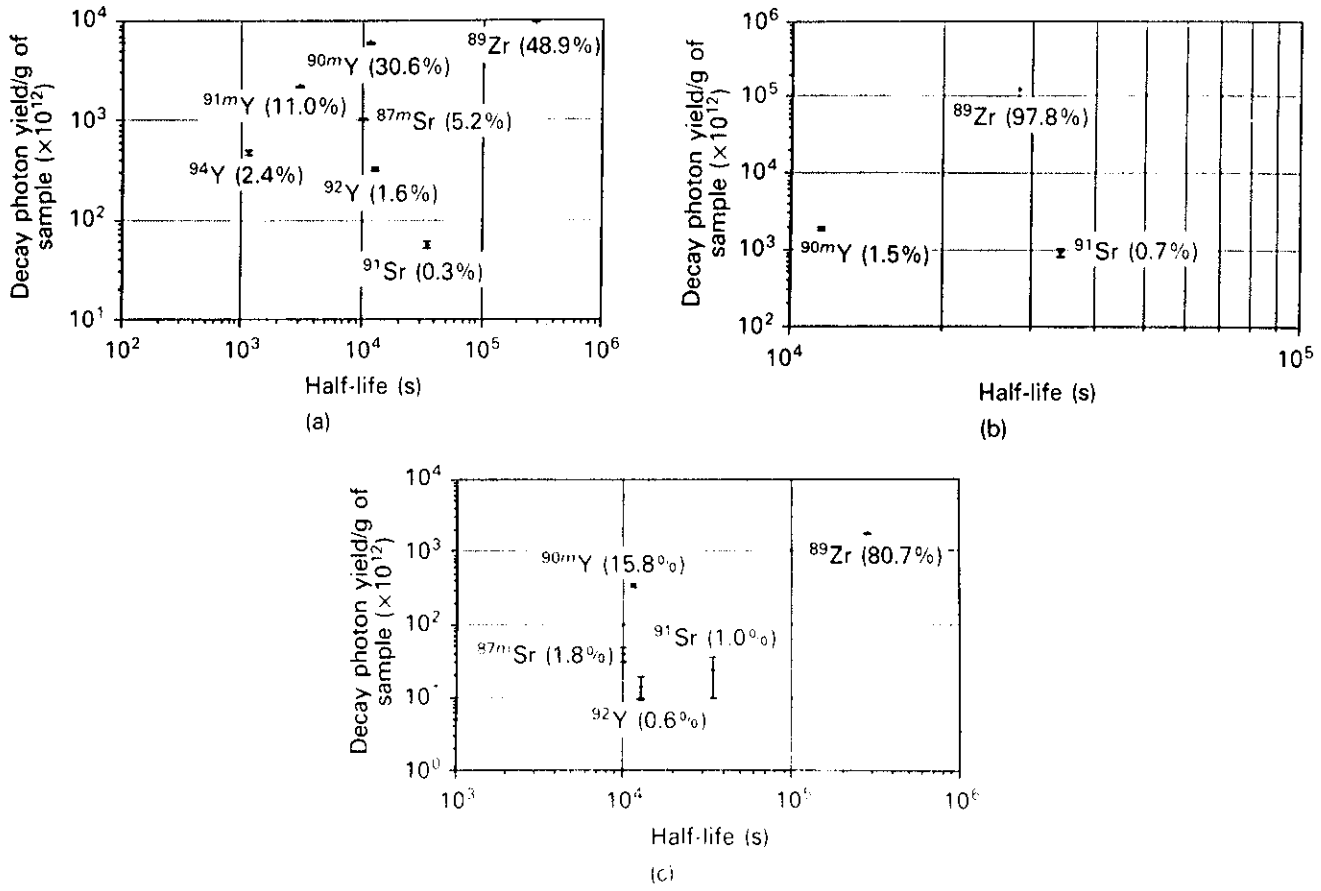

Fig. 5. Decay rates as a function of half-lives of products resulting from fusion-neutron irradiation to a zirconium sample at 10-cm spectrum for (a) T_i = 30 min and T_c = 56.5 min and for (b) T_i = 9 h and T_c = 17 h, 15.7 min; and (c) at 82-cm spectrum for T_i = 10 h and T_c = 3 h, 13.5 min.

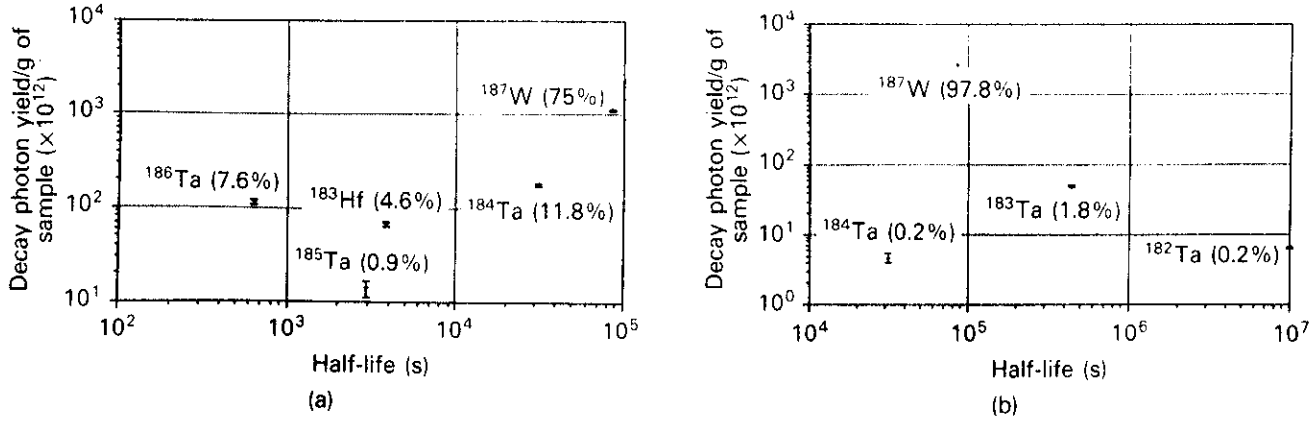

Fig. 6. Decay rates as a function of half-lives of products resulting from fusion-neutron irradiation to a tungsten sample at 10-cm spectrum for (a) T_i = 30 min and T_c = 37.3 min and for (b) T_i = 9 h and T_c = 2 days, 19 h, 3.5 min.

decay and cross-section data used in DKRICF is discussed when needed. Detailed explanations on observed discrepancies are summarized in the following for each material.

IV.A. Zirconium

It was found that ^{89}Zr, ^{89m}Zr, ^{90m}Y, ^{87m}Sr, and ^{91m}Y are major contributors to the decay photons,

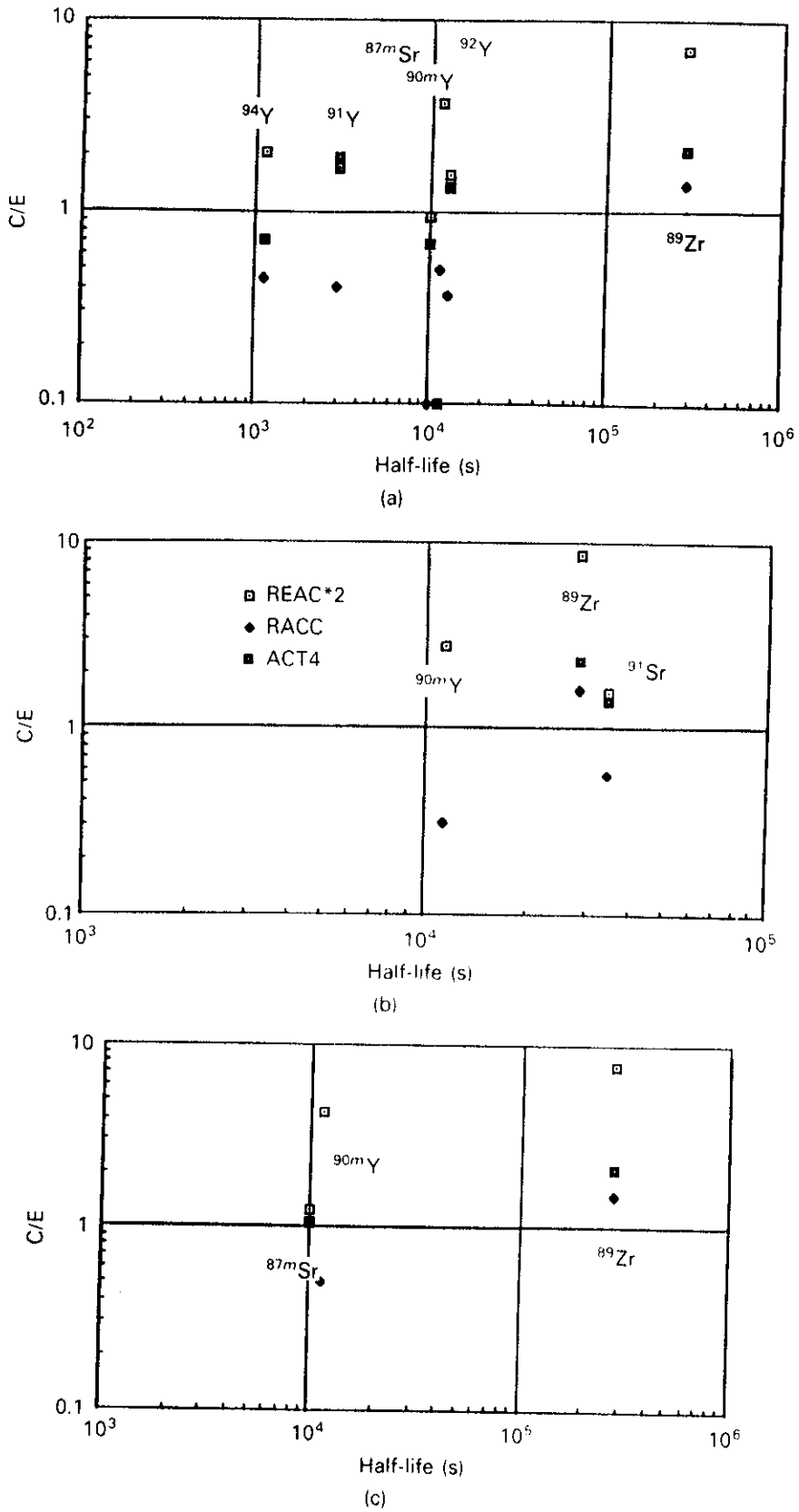

Fig. 7. Decay rate C/E ratios as a function of half-lives of products for zirconium sample at 10-cm spectrum for (a) T_r = 30 min and T_c = 56.5 min and for (b) T_r = 9 h and T_c = 17 h, 15.7 min; and (c) at 82-cm spectrum for T_r = 10 h and T_c = 3 h, 13.5 min.

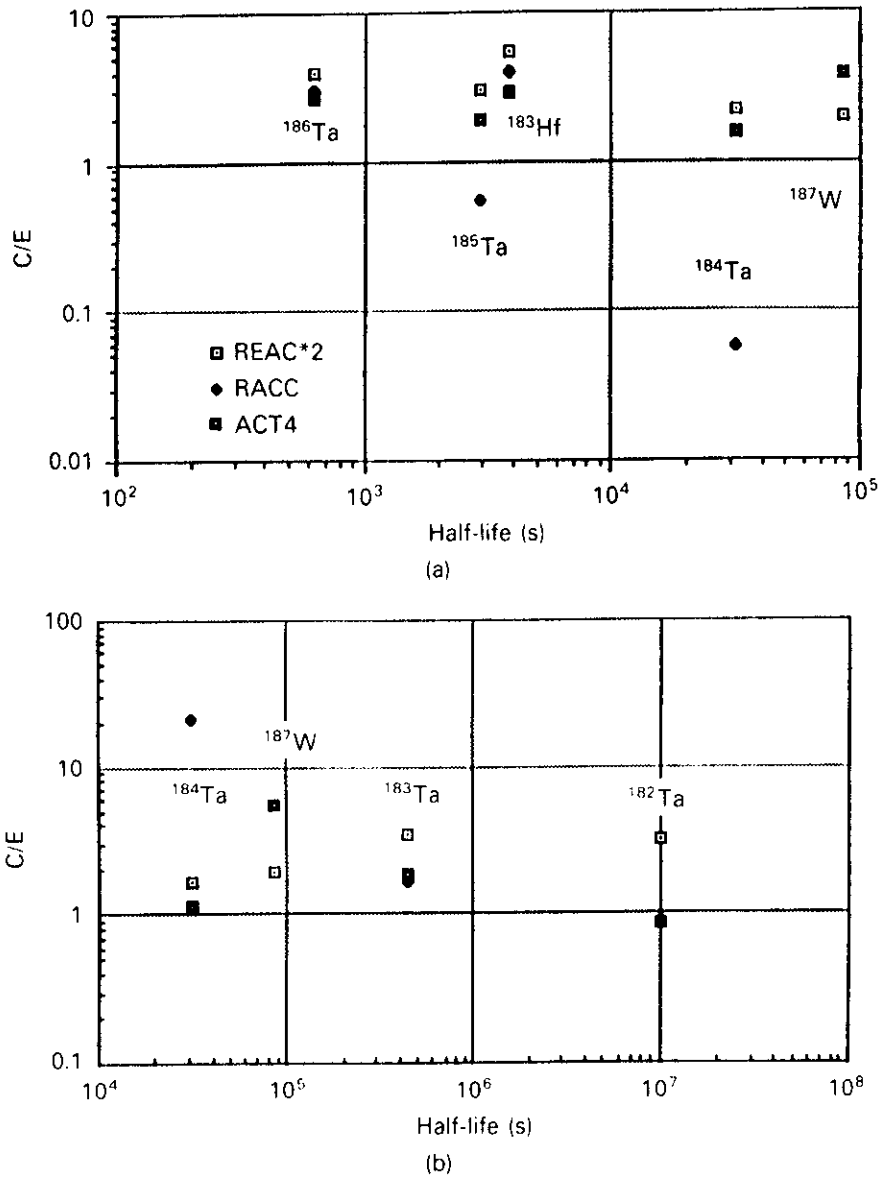

Fig. 8. Decay rate C/E ratios as a function of half-lives of products for tungsten sample at 10-cm spectrum for (a) T_r = 30 min and T_c = 37.3 min and for (b) T_r = 9 h and T_c = 2 days, 19 h, 3.5 min.

and correspondingly, $^{90}Zr(n,2n)$, $^{90}Zr(n,2n)^m$, $^{90}Zr(n,p)^m$, $^{90}Zr(n,\alpha)^m$, and $^{91}Zr(n,p)^m$ are the most important reactions. Minor contributors include ^{91}Y, ^{92}Y, ^{94}Y, and ^{91}Sr.

IV.A.1. Decay Data

Observations on the decay data relevant to the nuclides mentioned in Sec. IV.A can be summarized as follows:

1. All four codes have one common fault in the zirconium-related decay data: the overestimation of decay photons from ^{89}Zr in the 0.4- to 1.0-MeV energy bin by including 1.44 γ/decay instead of 0.99 γ/decay as in the Table of Radioactive Isotopes[54] or the Table of Isotopes.[55]

2. The REAC*2 and ACT4 codes overestimate the production of the 909-keV photon from ^{89}Zr by counting this photon twice. Once ^{89}Zr is formed, it decays into ^{89m}Y, and then ^{89m}Y decays into its ground state by emitting 909-keV photons, as shown in Fig. 9, which depicts the decay scheme of ^{89}Zr and ^{89m}Zr. However, REAC*2 and ACT4 treat this situation as ^{89}Zr decaying into ^{89m}Y by emitting 909-keV photons and as ^{89m}Y decaying into its ground state by emitting another 909-keV photon, which is obviously wrong. Because there is no reaction channel for the production

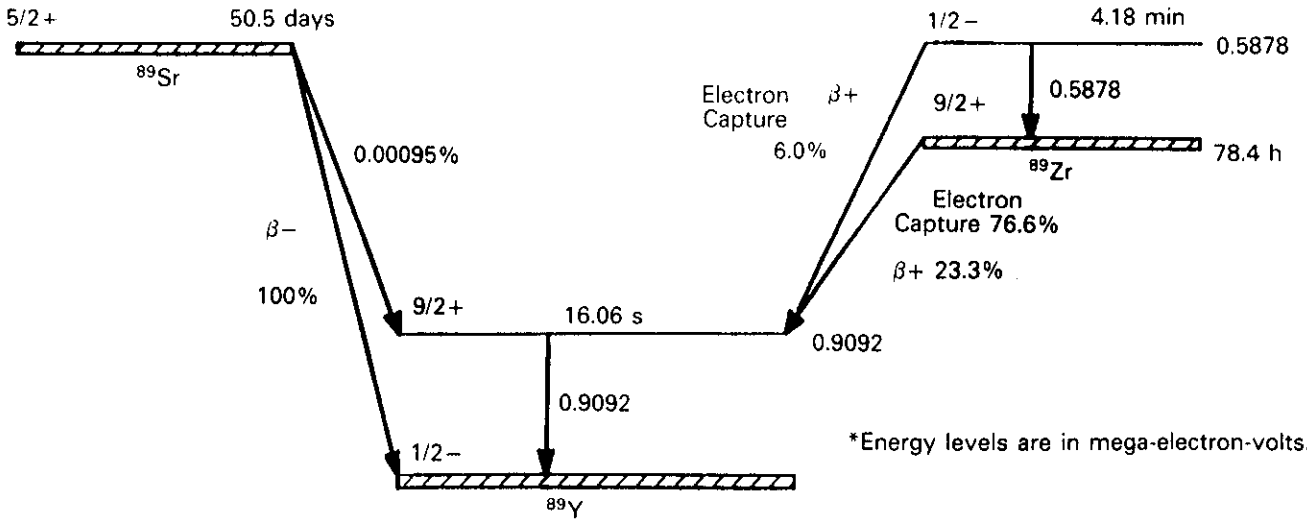

Fig. 9. Decay scheme for ^{89}Zr, ^{89m}Zr, and ^{89}Sr (taken from Table of Isotopes,[55] 7th edition).

of ^{89}Sr, it would not contribute to the observed 909-keV photon yield in our case.

3. The REAC*2 code includes two wrong photon emission probabilities for ^{94}Y, in the 0.4- to 1.0-MeV and 1.0- to 1.5-MeV energy bins. It has 0.83 γ/decay instead of 0.63 γ/decay in the former bin and 0.1 γ/decay instead of 0.077 γ/decay in the latter bin.

4. The RACC code does not include any decay data for ^{87m}Sr.

5. The RACC and DKRICF codes have wrong decay photon emission data for ^{94}Y, ^{91}Y, and ^{91}Sr, while ACT4 does not have any major problems with these nuclides. RACC and DKRICF have 0.49 γ/decay instead of 0.63 γ/decay in the 0.4- to 1.0-MeV bin, 0.05 γ/decay instead of 0.075 γ/decay in the 1.0- to 1.5-MeV bin, and 0.04 γ/decay instead of 0.028 γ/decay in the 1.5- to 2.0-MeV bin. For ^{92}Y, RACC and DKRICF include the wrong photon emission probability of 0.63 γ/decay instead of 0.21 γ/decay in the 0.4- to 1.0-MeV energy bin. For ^{91}Sr, RACC and DKRICF both have 0.48 γ/decay in the 0.4- to 1.0-MeV bin instead of 1.04 γ/decay as in the Table of Radioactive Isotopes. Immediate correction is desirable even though the contributions of these nuclides to the total decay rates are negligible.

6. The ACT4 code lacks decay data for ^{90m}Y.

IV.A.2. Cross-Section Data

Most of the cross sections relevant to zirconium do not seem to be adequate. Among those, the most notorious cross sections are for the ^{90}Zr$(n,2n)^{89m}$Zr and ^{90}Zr$(n,p)^{90m}$Y reactions, depicted in Figs. 10 and 11, respectively. In these figures, the experimental data are compared with the cross sections extracted from the codes. Differences of one or two orders of magnitude were found. The major problems observed are as follows:

1. The REAC*2 code overestimates the cross sections for reactions leading to isomeric-state products by calculating them as being of the same magnitude as those for reactions leading to ground-state products. For example, REAC*2 has same cross sections for both ^{90}Zr$(n,p)^{90g}$Y and ^{90}Zr$(n,p)^{90m}$Y. This leads to an overestimate of the production of ^{89m}Zr, ^{90m}Y, ^{87m}Sr, and ^{91m}Y.

2. The RACC code does not have the cross section for the ^{90}Zr$(n,\alpha)^{87m}$Sr reaction.

3. The ACT4 version that we used in this study does not include the cross section for the ^{90}Zr$(n,p)^{90m}$Y reaction.

IV.B. Tungsten

For tungsten, it was observed that the following reactions and their products are the most important in terms of emitting decay photons: ^{186}W$(n,\gamma)^{187}$W, ^{186}W$(n,p)^{186}$Ta, ^{186}W$(n,np/d)^{185}$Ta, ^{184}W$(n,p)^{184}$Ta, ^{183}W$(n,p)^{183}$Ta, ^{182}W$(n,p)^{182}$Ta, and ^{186}W$(n,\alpha)^{183}$Hf.

IV.B.1. Decay Data

The status of decay data pertinent to the nuclides listed in Sec. IV.B can be discussed as follows:

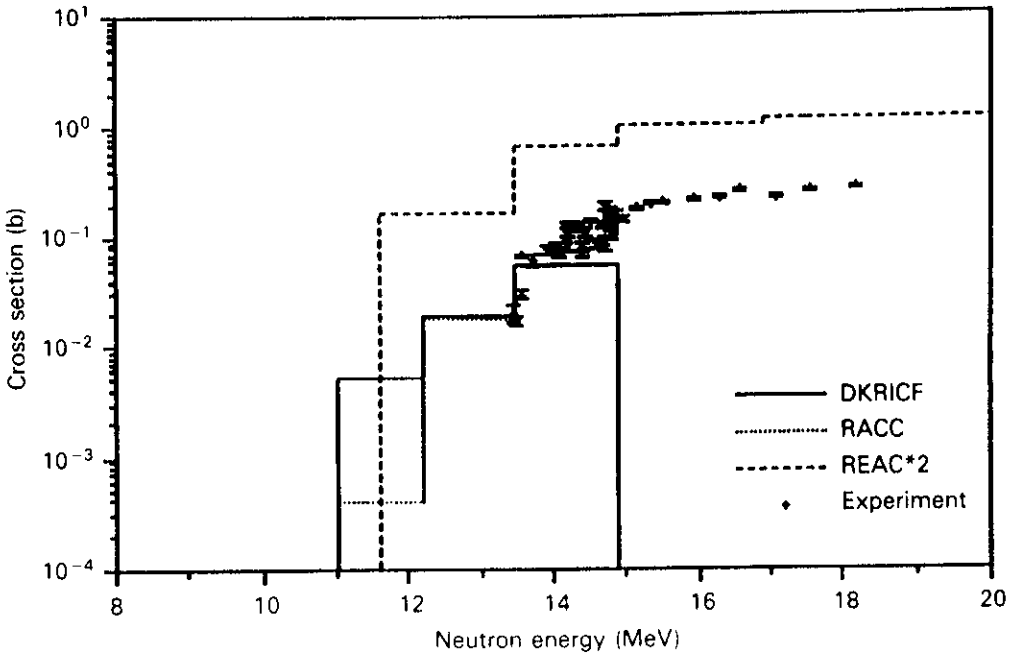

Fig. 10. Cross section for $^{90}Zr(n,2n)^{89m}Zr$ reaction.

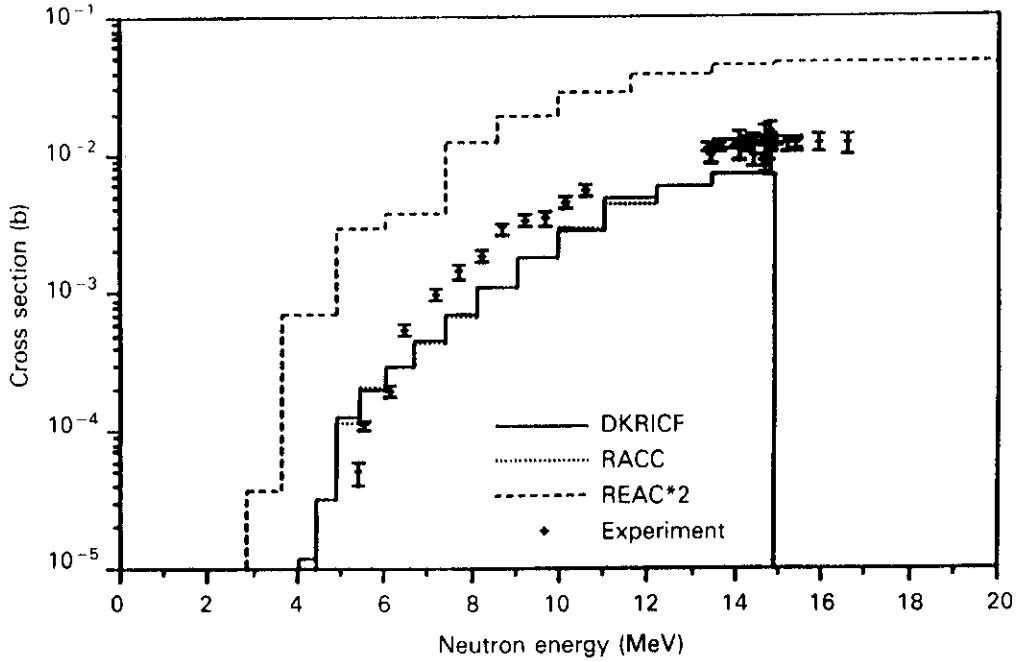

Fig. 11. Cross section for $^{90}Zr(n,p)^{90m}Y$ reaction.

1. The REAC*2 code does not have any major errors in decay data for these nuclides. Even though it was not shown in the C/E analysis, however, REAC*2 has one major flaw in that it includes a totally wrong decay photon emission probability for ^{179m}W ($T_{1/2}$ = 6.4 min): ~4200 γ/decay instead of ~0.1 γ/decay as in the Table of Radioactive Isotopes. Hence, REAC*2 heavily overestimates the contribution of ^{179m}W in the case of a shorter cooling time.

2. The RACC and DKRICF codes have several problems:

a. The ^{184}Ta half-life is 7.519×10^5 s instead of 3.132×10^4 s.

b. The ^{186}Ta half-life is 6301.0 s instead of 630.0 s.

c. The decay photon emission data of ^{187}W in RACC are mistakenly interchanged with those of ^{186}W, which is a stable nuclide, so that no photons are assigned to ^{187}W.

d. There are inadequate (wrong or missing) photon emission data for virtually all the nuclides listed earlier.

3. The ACT4 code has a few problems:

a. the total absence of decay photons below 400 keV for ^{182}Ta

b. large discrepancies for two major decay photons from ^{187}W; that is, 0.83 γ/decay compared with 0.0035 γ/decay in the Table of Radioactive Isotopes for the 239-keV photon and 0.83 γ/decay compared with 0.087 γ/decay in the Table of Radioactive Isotopes for the 114-keV photon.

IV.B.2. Cross-Section Data

It was noted that the cross sections for all the reactions listed in Sec. IV.B seem to be overestimated in all of the codes. For example, the cross sections for the ^{186}W(n,p), ^{186}W(n,α), and ^{184}W(n,p) reactions used in the codes are compared with the ENDF/B-VI data library in Figs. 12, 13, and 14. Obviously, the values in the codes are overestimated.

V. IMPROVEMENT OF DECAY DATA

The decay data library of RACC has been modified. RACC was chosen from among the four codes mainly for the following two reasons: RACC can treat the pointwise representation of the decay photon spectrum, and it is being used as a major tool for decay heat calculations for the ITER blanket/shield design.[33] Hence, the improvement of the decay data in RACC has a direct application. Nevertheless, the data in the other codes can easily be modified or improved, depending on the user's particular interest in those codes.

The maximum number of distinct decay photons per single nuclide has been increased from 9 to 50. Because 50 distinct photons per nuclide are allowed, it was possible to include almost every photon emitted from the nuclides relevant to this study. Then, the half-lives and decay photon emission probabilities were extracted from the Table of Radioactive Isotopes and implemented into the RACC decay data library. The nuclides whose decay data have been modified are ^{89}Zr, ^{89m}Zr, ^{89m}Y, ^{90m}Y, ^{91m}Y, ^{92}Y, ^{94}Y, ^{87m}Sr, and ^{91}Sr for the zirconium case and ^{187}W, ^{186}Ta, ^{185}Ta, ^{184}Ta, ^{183}Ta, ^{182}Ta, and ^{183}Hf for the tungsten case. Table V shows

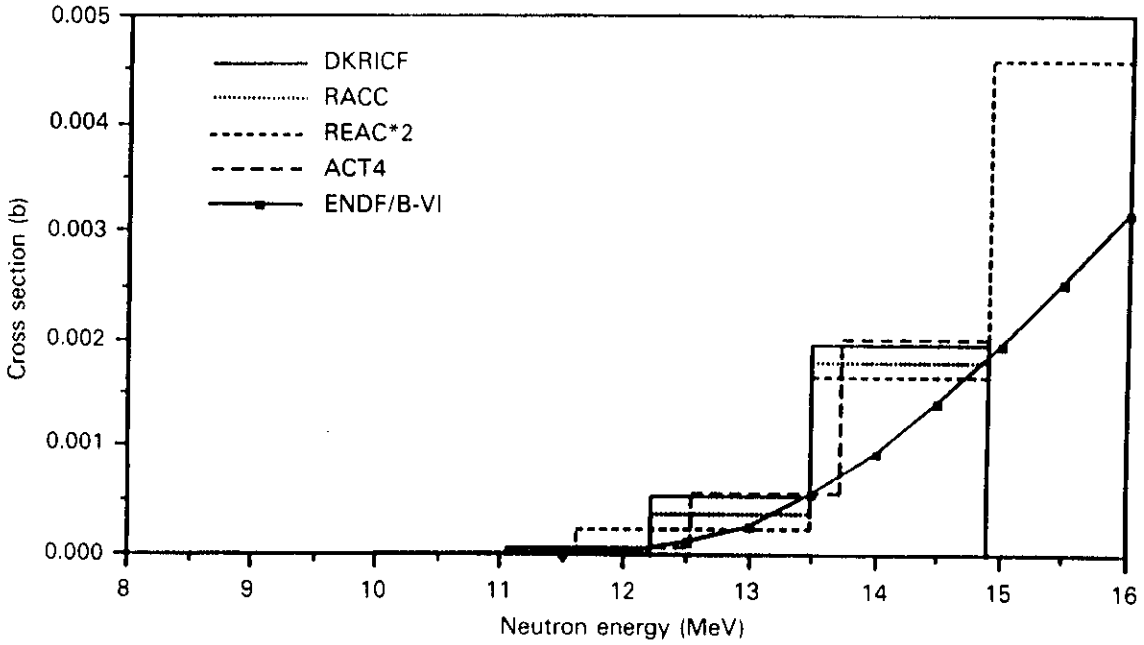

Fig. 12. Cross section for ^{186}W$(n,p)^{186}$Ta reaction.

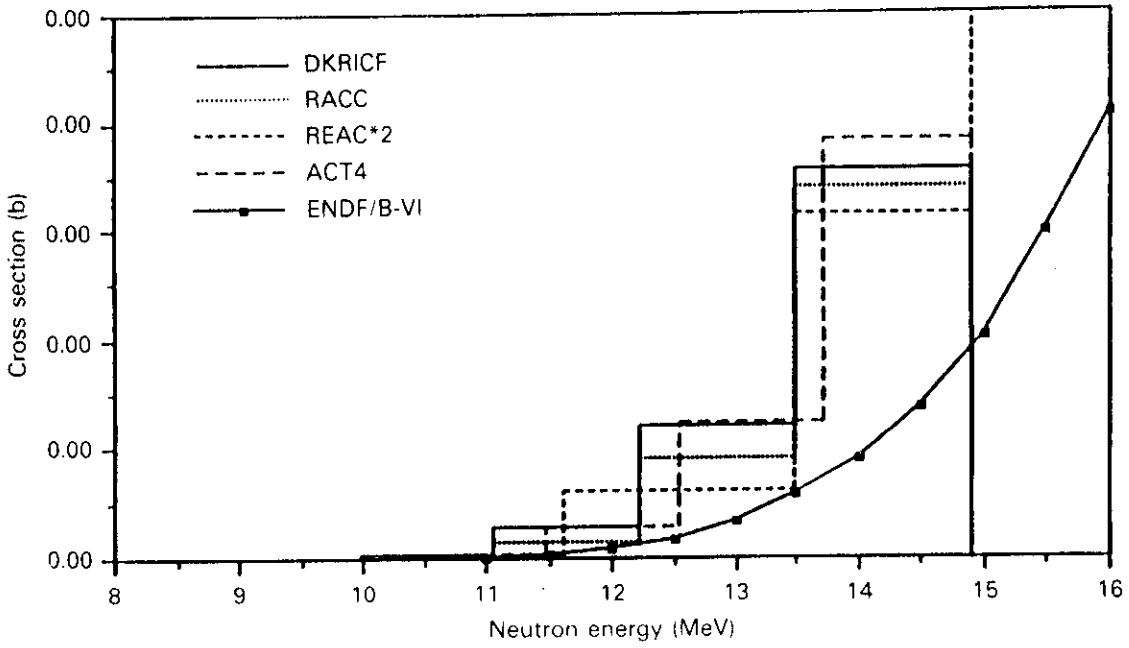

Fig. 13. Cross section for $^{186}W(n,\alpha)^{183}Hf$ reaction.

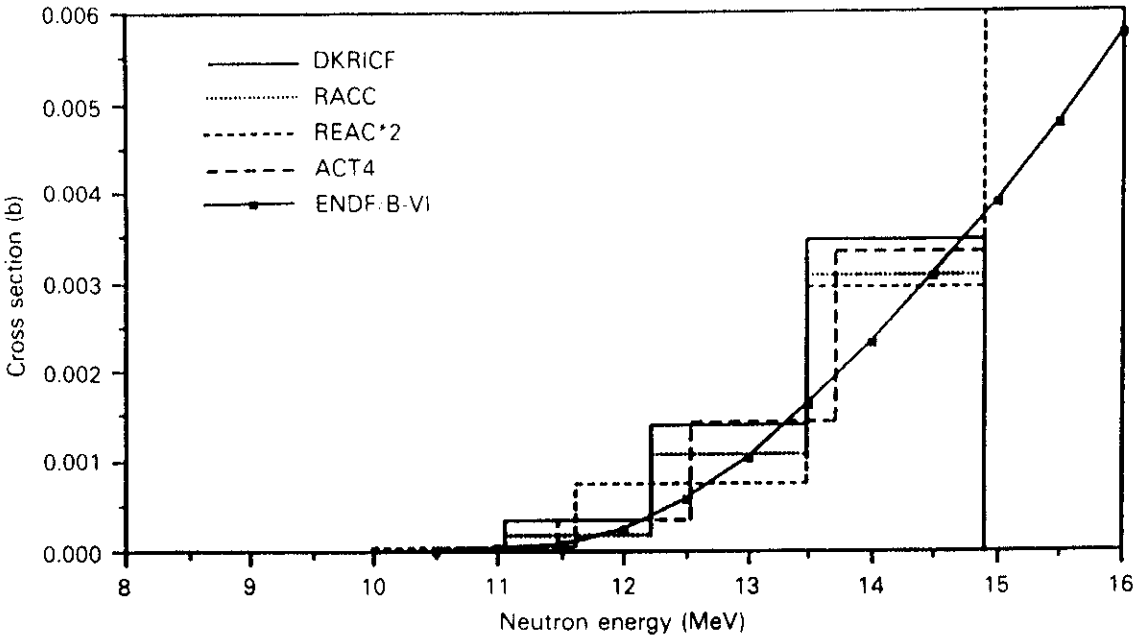

Fig. 14. Cross section for $^{184}W(n,p)^{184}Ta$ reaction.

the half-lives and decay photon spectrum data of these nuclides. The calculational results obtained by using the modified decay data have been compared with the experimentally measured decay photon yield. The new C/E ratios are presented later.

VI. IMPROVEMENT OF CROSS-SECTION DATA

Besides decay data, the transmutation cross sections are another major source of discrepancies between computed and measured decay rates. While the decay

TABLE V

Decay Photon Spectrum of the Major Nuclides Identified to be Important in the Analysis

Isotope	Half-Life	Photon Energy (keV) and Intensity (%)	Originating Reactions
^{87*}Sr	2.8 h	388.4 (82.3)	^{90}Zr$(n,\alpha)^*$
^{91}Sr	9.52 h	556 (61.5), 653 (8.0), 750 (23.6), 926 (3.84), 1024 (33)	^{92}Zr$(n,2p)$, ^{94}Zr(n,α)
^{89*}Y	16.06 s	909 (99.14)	^{90}Zr$(n,np)^*(n,d)^*$, ^{91}Zr$(n,t)^*$
^{90*}Y	3.19 h	202.5 (96.6), 479.5 (91)	^{90}Zr$(n,p)^*$, ^{91}Zr$(n,np)^*(n,d)^*$, ^{92}Zr$(n,t)^*$
^{91*}Y	49.7 min	556 (94.9)	^{91}Zr$(n,p)^*$, ^{92}Zr$(n,np)^*(n,d)^*$
^{92}Y	3.54 h	449 (2.34), 561 (2.4), 935 (13.9), 1405 (4.8)	^{92}Zr(n,p), ^{94}Zr(n,t)
^{94}Y	18.7 min	382 (2.02), 551 (4.9), 919 (56), 1139 (6.0)	^{94}Zr(n,p), ^{96}Zr(n,t)
^{89}Zr	3.27 days	909 (99), 1621 (0.07), 1657 (0.099), 1713 (0.76), 1745 (0.129)	^{90}Zr$(n,2n)$
^{89*}Zr	4.18 min	588 (89.5), 1507 (6.04)	^{90}Zr$(n,2n)^*$
^{183}Hf	1.067 h	73.173 (38), 397.86 (2.9), 459.07 (27), 783.75 (65), 1470.2 (2.7)	^{184}W$(n,2p)$, ^{186}W(n,α)
^{182}Ta	115 days	67.75 (41.2), 100.1 (14.0), 1121.3 (34.7), 1189.1 (16.5), 1221.4 (27.3), 1231.0 (11.6)	^{182}W(n,p), ^{183}W$(n,np)(n,d)$, ^{184}W(n,t)
^{183}Ta	5.1 days	99.1 (6.5), 107.9 (10.7), 144.1 (2.47), 161.3 (8.8), 246.06 (28), 291.7 (3.8), 313.0 (3.32), 354.0 (11.36)	^{183}W(n,p), ^{184}W$(n,np)(n,d)$
^{184}Ta	8.7 h	111.21 (24.3), 215.33 (11.4), 252.85 (44), 318.01 (23.5), 384.26 (12.8), 414.04 (73.9), 461.04 (10.9), 536.68 (13.2), 792.07 (15.0), 894.76 (11.0), 903.28 (15.3), 920.94 (32.6)	^{184}W(n,p), ^{186}W(n,t)
^{185}Ta	49 min	173.68 (22), 177.39 (25.6)	^{186}W$(n,np)(n,d)$
^{186}Ta	10.5 min	122.43 (23), 198.05 (59), 215.0 (49.9), 307.66 (11.4), 418.0 (14.8), 510.68 (44)	^{186}W(n,p)
^{179*}W	6.4 min	221.95 (8.6)	^{180}W$(n,2n)^*$
^{187}W	23.9 h	71.98 (10.8), 114.0 (0.074), 134.23 (8.56), 207 (0.138), 239 (0.083), 479.53 (21.1), 551.52 (4.92), 589 (0.118), 618.34 (6.07), 682 (0.013), 685.74 (26.4), 745 (0.288), 772.89 (3.98), 865 (0.325), 880 (0.137)	^{186}W(n,γ)

data were corrected by using a standard reference such as the Table of Radioactive Isotopes, the cross sections are relatively difficult to improve, largely because of the lack of such a standard. For example, one might consider ENDF/B-V (Ref. 56) or ENDF/B-VI (Ref. 53) as a standard. However, those are not appropriate for our study, especially for the zirconium sample case, because ENDF does not have separate cross sections for the reactions that lead to the isomeric-state product. For zirconium, most of the concern lies in the improvement of the cross sections for the isomeric-state products.

A very simple curve-fitting procedure to represent the measured cross sections was developed. Our fitting formula began with the close examination of ACTL systematics,[57] which was developed in the late 1970s. One of the advantages over the original ACTL work can be credited to the much more extensive collection of experimentally measured cross sections over wide energy ranges that are now available. In addition to the simple physical considerations, the fitting formula was designed to follow the experimental trends of the excitation function. The physical considerations are that the cross section should be zero when the incident neutron energy is equal to or less than the threshold energy and that the rising portion of the excitation function for any threshold reaction generally has a sigmoid shape. Note that our interest lies in the threshold reactions, so that the method developed here will operate only on those reactions.

The following equation has been proposed, inspired by the ACTL formulation:

$$\sigma(E_n) = \sigma(plat.)\{1.0 - \exp[-f(x)]\} , \qquad (2)$$

where

$\sigma(plat.)$ = cross section at plateau, usually taken from experimental data

E_{th} = threshold energy

$x \equiv E_n - E_{th}$

$f(x)$ = polynomial in x of degree m. (Note that in ACTL only a quadratic in x appears in its exponent.) In other words, $f(x)$ is defined as

$$f(x) \equiv \sum_{m=1} a_m x^m = \sum_{m=1} a_m (E_n - E_{th})^m . \qquad (3)$$

Note that summation starts from $m = 1$, not $m = 0$, to give $\sigma(E_n = E_{th}) = 0.0$. Now, the remaining tasks are

TABLE V

Decay Photon Spectrum of the Major Nuclides Identified to be Important in the Analysis

Isotope	Half-Life	Photon Energy (keV) and Intensity (%)	Originating Reactions
^{87*}Sr	2.8 h	388.4 (82.3)	^{90}Zr$(n,\alpha)^*$
^{91}Sr	9.52 h	556 (61.5), 653 (8.0), 750 (23.6), 926 (3.84), 1024 (33)	^{92}Zr$(n,2p)$, ^{94}Zr(n,α)
^{89*}Y	16.06 s	909 (99.14)	^{90}Zr$(n,np)^*(n,d)^*$, ^{91}Zr$(n,t)^*$
^{90*}Y	3.19 h	202.5 (96.6), 479.5 (91)	^{90}Zr$(n,p)^*$, ^{91}Zr$(n,np)^*(n,d)^*$, ^{92}Zr$(n,t)^*$
^{91*}Y	49.7 min	556 (94.9)	^{91}Zr$(n,p)^*$, ^{92}Zr$(n,np)^*(n,d)^*$
^{92}Y	3.54 h	449 (2.34), 561 (2.4), 935 (13.9), 1405 (4.8)	^{92}Zr(n,p), ^{94}Zr(n,t)
^{94}Y	18.7 min	382 (2.02), 551 (4.9), 919 (56), 1139 (6.0)	^{94}Zr(n,p), ^{96}Zr(n,t)
^{89}Zr	3.27 days	909 (99), 1621 (0.07), 1657 (0.099), 1713 (0.76), 1745 (0.129)	^{90}Zr$(n,2n)$
^{89*}Zr	4.18 min	588 (89.5), 1507 (6.04)	^{90}Zr$(n,2n)^*$
^{183}Hf	1.067 h	73.173 (38), 397.86 (2.9), 459.07 (27), 783.75 (65), 1470.2 (2.7)	^{184}W$(n,2p)$, ^{186}W(n,α)
^{182}Ta	115 days	67.75 (41.2), 100.1 (14.0), 1121.3 (34.7), 1189.1 (16.5), 1221.4 (27.3), 1231.0 (11.6)	^{182}W(n,p), ^{183}W$(n,np)(n,d)$, ^{184}W(n,t)
^{183}Ta	5.1 days	99.1 (6.5), 107.9 (10.7), 144.1 (2.47), 161.3 (8.8), 246.06 (28), 291.7 (3.8), 313.0 (3.32), 354.0 (11.36)	^{183}W(n,p), ^{184}W$(n,np)(n,d)$
^{184}Ta	8.7 h	111.21 (24.3), 215.33 (11.4), 252.85 (44), 318.01 (23.5), 384.26 (12.8), 414.04 (73.9), 461.04 (10.9), 536.68 (13.2), 792.07 (15.0), 894.76 (11.0), 903.28 (15.3), 920.94 (32.6)	^{184}W(n,p), ^{186}W(n,t)
^{185}Ta	49 min	173.68 (22), 177.39 (25.6)	^{186}W$(n,np)(n,d)$
^{186}Ta	10.5 min	122.43 (23), 198.05 (59), 215.0 (49.9), 307.66 (11.4), 418.0 (14.8), 510.68 (44)	^{186}W(n,p)
^{179*}W	6.4 min	221.95 (8.6)	^{180}W$(n,2n)^*$
^{187}W	23.9 h	71.98 (10.8), 114.0 (0.074), 134.23 (8.56), 207 (0.138), 239 (0.083), 479.53 (21.1), 551.52 (4.92), 589 (0.118), 618.34 (6.07), 682 (0.013), 685.74 (26.4), 745 (0.288), 772.89 (3.98), 865 (0.325), 880 (0.137)	^{186}W(n,γ)

data were corrected by using a standard reference such as the Table of Radioactive Isotopes, the cross sections are relatively difficult to improve, largely because of the lack of such a standard. For example, one might consider ENDF/B-V (Ref. 56) or ENDF/B-VI (Ref. 53) as a standard. However, those are not appropriate for our study, especially for the zirconium sample case, because ENDF does not have separate cross sections for the reactions that lead to the isomeric-state product. For zirconium, most of the concern lies in the improvement of the cross sections for the isomeric-state products.

A very simple curve-fitting procedure to represent the measured cross sections was developed. Our fitting formula began with the close examination of ACTL systematics,[57] which was developed in the late 1970s. One of the advantages over the original ACTL work can be credited to the much more extensive collection of experimentally measured cross sections over wide energy ranges that are now available. In addition to the simple physical considerations, the fitting formula was designed to follow the experimental trends of the excitation function. The physical considerations are that the cross section should be zero when the incident neutron energy is equal to or less than the threshold energy and that the rising portion of the excitation function for any threshold reaction generally has a sigmoid shape. Note that our interest lies in the threshold reactions, so that the method developed here will operate only on those reactions.

The following equation has been proposed, inspired by the ACTL formulation:

$$\sigma(E_n) = \sigma(plat.)\{1.0 - \exp[-f(x)]\} , \qquad (2)$$

where

$\sigma(plat.)$ = cross section at plateau, usually taken from experimental data

E_{th} = threshold energy

$x \equiv E_n - E_{th}$

$f(x)$ = polynomial in x of degree m. (Note that in ACTL only a quadratic in x appears in its exponent.) In other words, $f(x)$ is defined as

$$f(x) \equiv \sum_{m=1} a_m x^m = \sum_{m=1} a_m (E_n - E_{th})^m . \qquad (3)$$

Note that summation starts from $m = 1$, not $m = 0$, to give $\sigma(E_n = E_{th}) = 0.0$. Now, the remaining tasks are

to decide when to terminate the series and then to determine the coefficients a_m that result in the best fit with experimental data. Since the trend or shape of the excitation functions greatly varies by reaction type, no effort has been made to standardize the procedure for determining the maximum order of the polynomial. The termination of the series totally depends on the accuracy limit chosen by the users based on their needs. But, as will be seen shortly, it can be said that in general the maximum orders lie between 3 and 7. A simple least-squares method with a covariance matrix was used to determine the coefficients a_m after the maximum order was set.

The polynomial formulation was applied to reactions such as $^{27}Al(n,\alpha)$, $^{58}Ni(n,2n)$, $^{90}Zr(n,2n)^{g+m}$, $^{90}Zr(n,2n)^{m}$, $^{90}Zr(n,p)^{m}$, $^{90}Zr(n,\alpha)^{m}$, $^{91}Zr(n,p)^{m}$, $^{186}W(n,p)$, $^{186}W(n,\alpha)$, $^{186}W(n,np)$, $^{184}W(n,p)$, $^{183}W(n,p)$, and $^{182}W(n,p)$. The first two reactions were included to validate the procedure used in this work by applying the method to well-known standard reactions. For the $^{27}Al(n,\alpha)$ reaction, the experimental data by Butler and Santry,[58] Liskien and Paulsen,[59] and Paulsen and Liskien[60] were used for the curve fitting. These measurement data were also used in the ENDF/B-VI evaluation, so that a direct validation of the fitting method can be made. As shown in Fig. 15, the excitation function that was obtained represents the experimental data very well as does ENDF/B-VI. Figure 16 compares our fitting result with the ENDF/B-VI data for the $^{58}Ni(n,2n)$ reaction. The figure also shows representative experimental data from Ikeda et al.[61] and Pavlik et al.[62] It seems that the fitting curve represents the experimental data better than ENDF/B-VI does for this reaction. The two reactions are very well studied standard reactions, which validate the fitting procedure.

Figures 17 through 21 show the results of the curve fitting for the reactions pertinent to the zirconium sample. Figures 22 through 27 display the results for the tungsten case, where ENDF/B-VI data were used for the curve fitting instead of experimental data because of the lack of experimental data for those reactions. It has been assumed that the ENDF/B-VI data have a 5% error at every point during the curve fitting. The fitting results are summarized in Table VI. An interested user can easily reproduce the excitation functions with the information listed there.

To quantify the quality of the fitting, a statistical measure of the goodness-of-fit was obtained by computing the χ^2 and the probability Q as follows[70]:

$$\chi^2 \equiv \sum_{i=1}^{n} \left[\frac{\sigma_{exp\,i} - \sigma_{sys}(x_i; a_1, \ldots, a_m)}{\delta\sigma_{exp\,i}} \right]^2 , \qquad (4)$$

where

$\delta\sigma_{exp\,i}$ = standard deviation of i'th experimental data

m = order of polynomial

n = number of experimental data

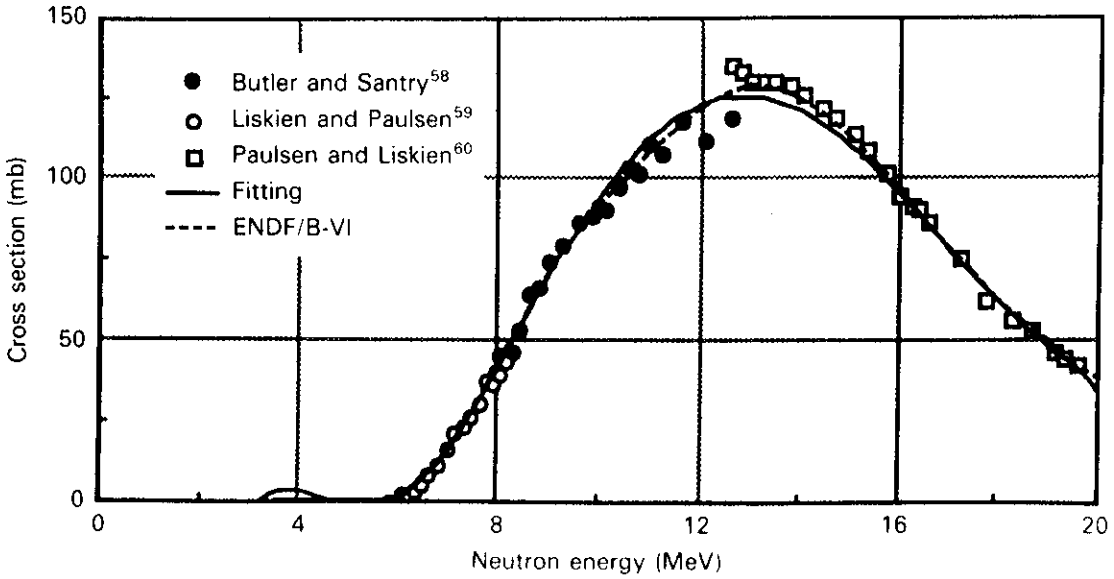

Fig. 15. Comparison of $^{27}Al(n,\alpha)$ reaction cross sections between ENDF/B-VI and the curve-fitting results. Representative experimental data are also included.

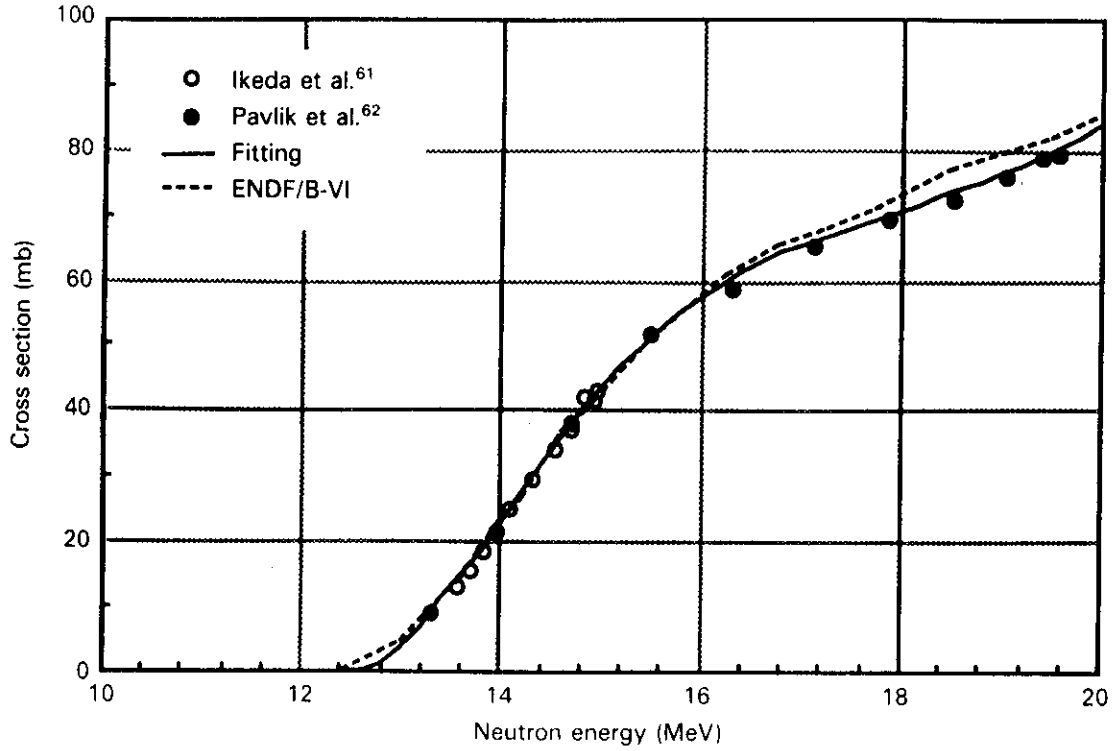

Fig. 16. Comparison of $^{58}Ni(n,2n)$ reaction cross sections between ENDF/B-VI and the curve-fitting results. Representative experimental data are also included.

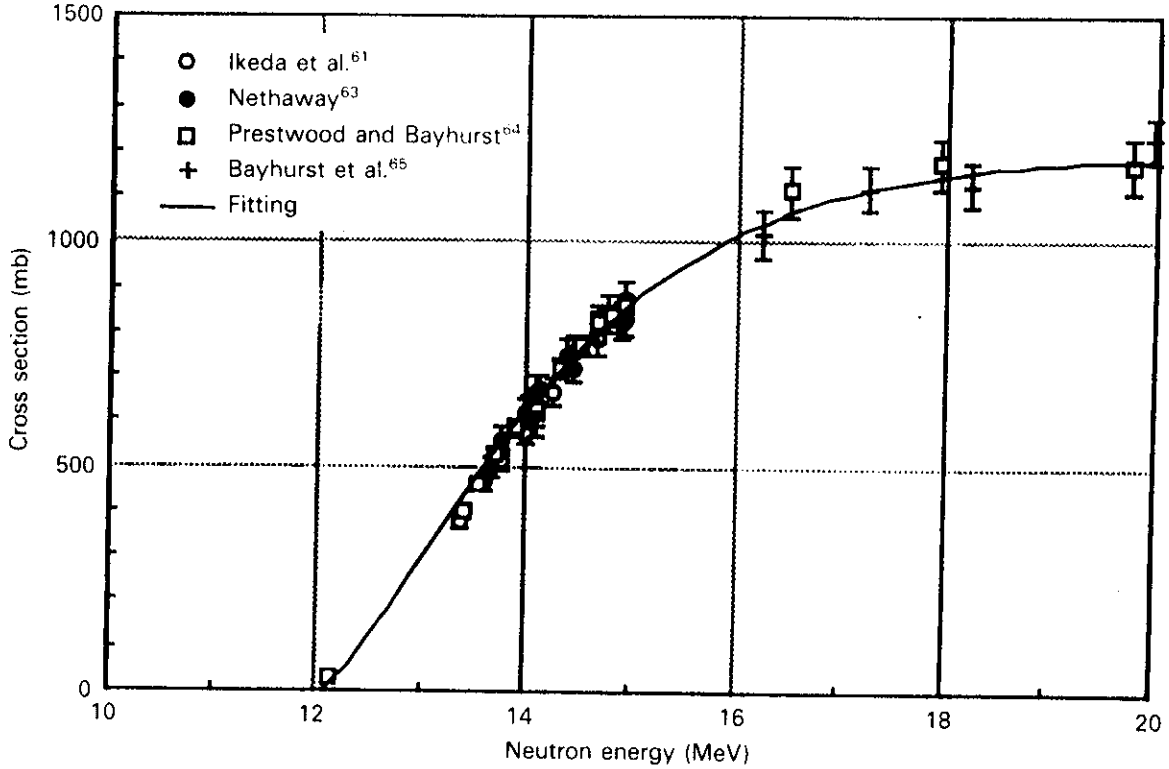

Fig. 17. Curve-fitting result for the $^{90}Zr(n,2n)$ reaction based on representative experimental data.

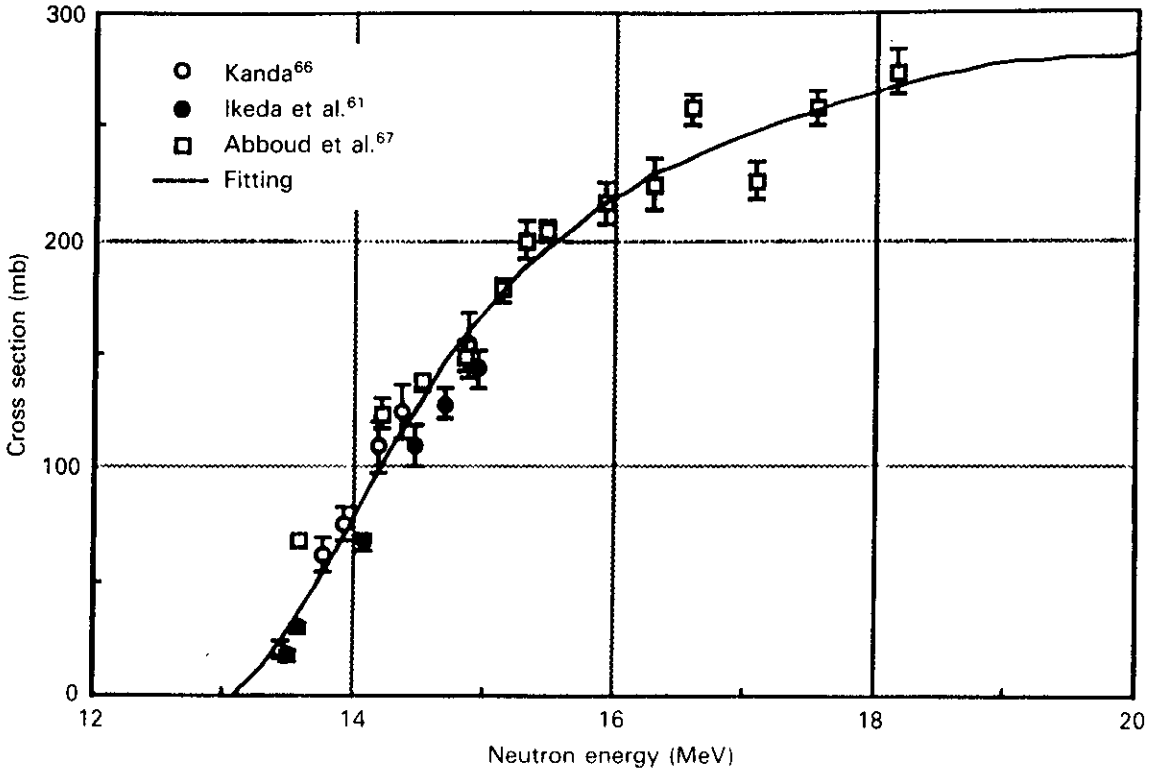

Fig. 18. Curve-fitting result for the $^{90}Zr(n,2n)^{m}$ reaction based on representative experimental data.

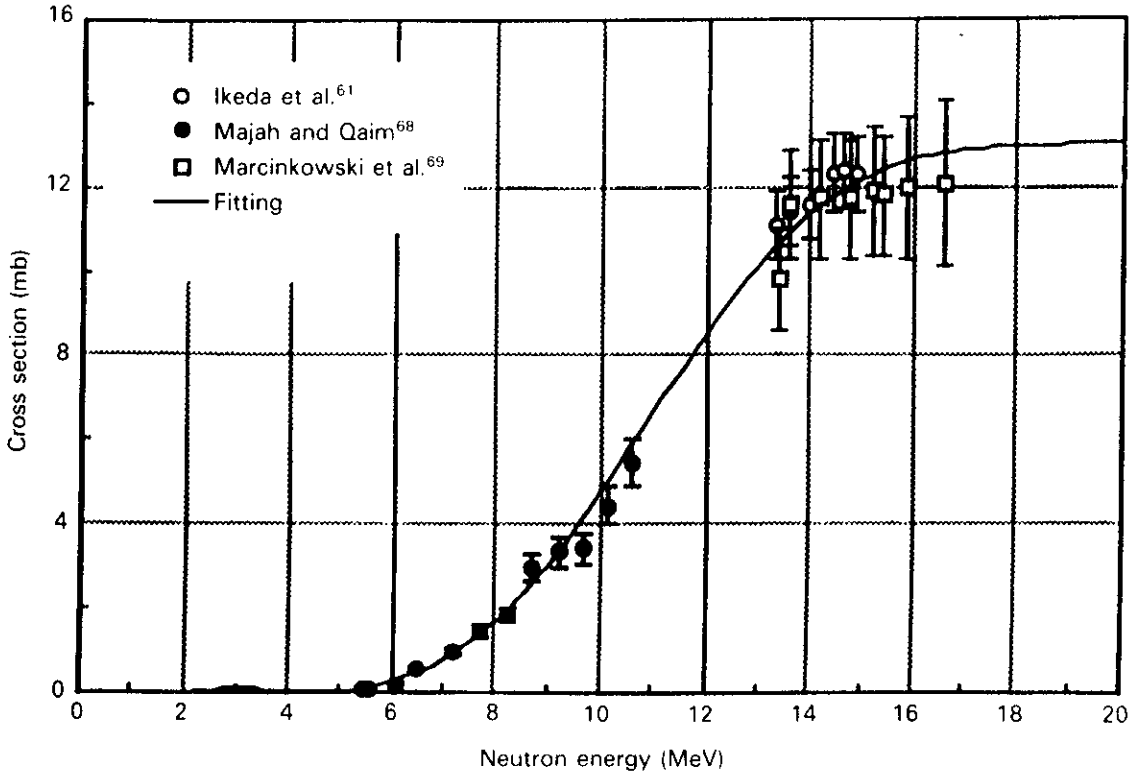

Fig. 19. Curve-fitting result for the $^{90}Zr(n,p)^{m}$ reaction based on representative experimental data.

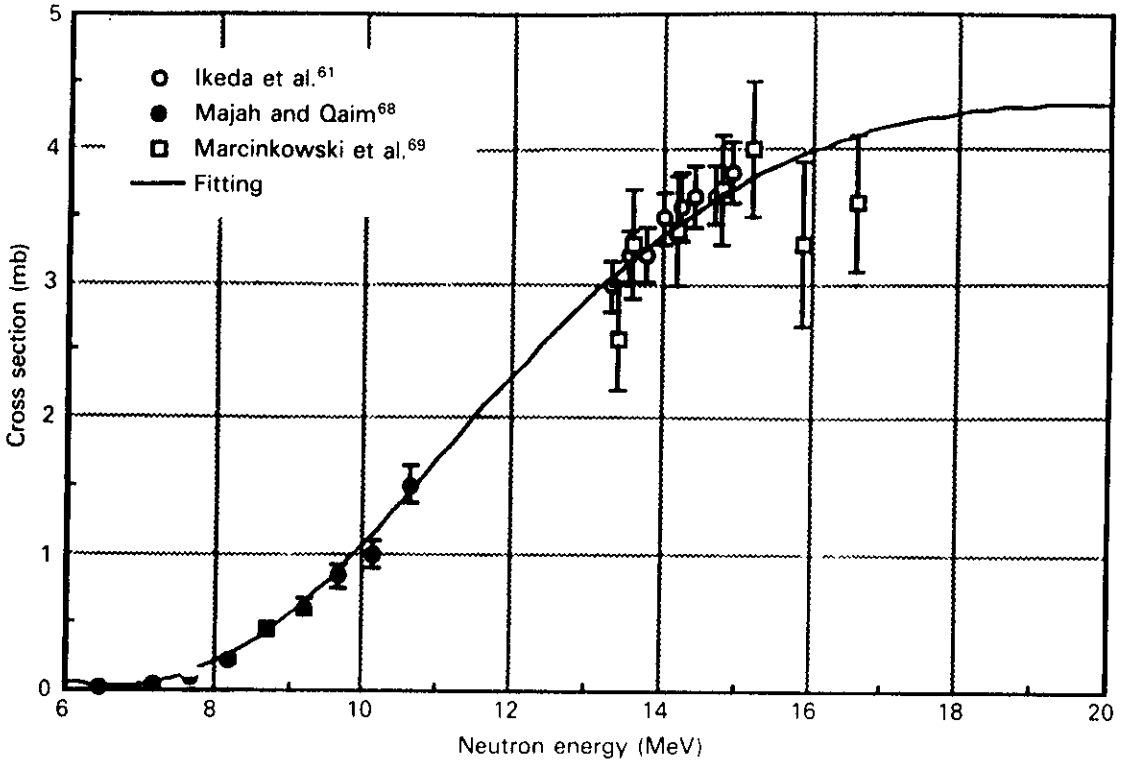

Fig. 20. Curve-fitting result for the $^{90}Zr(n,\alpha)^{m}$ reaction based on representative experimental data.

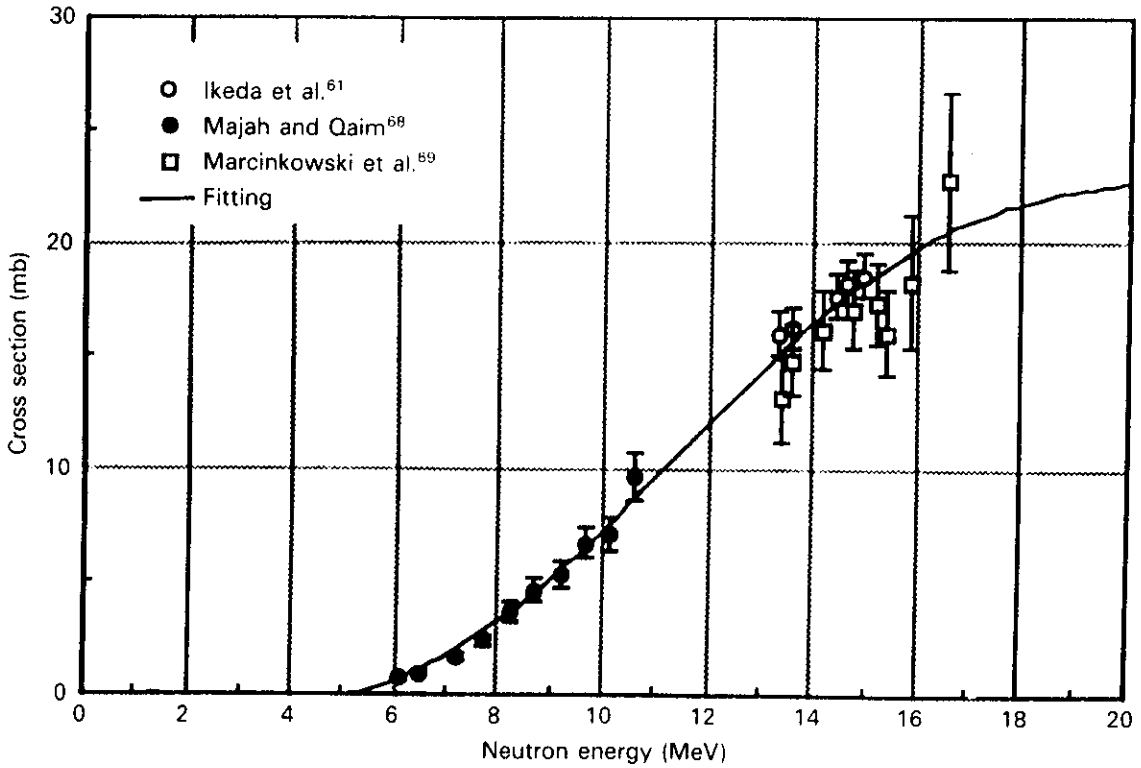

Fig. 21. Curve-fitting result for the $^{91}Zr(n,p)^{m}$ reaction based on representative experimental data.

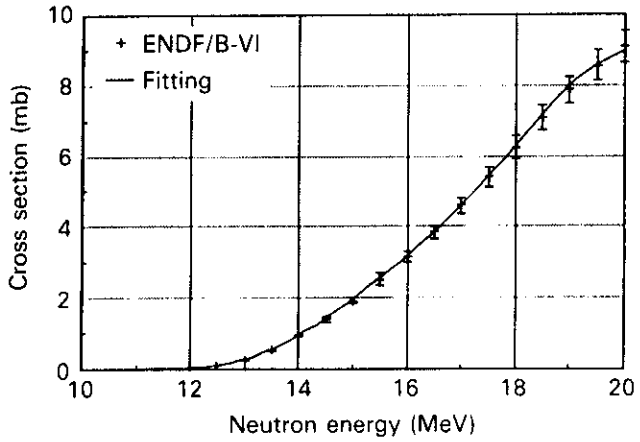

Fig. 22. Curve-fitting result for $^{186}W(n,p)$ reaction based on ENDF/B-VI data.

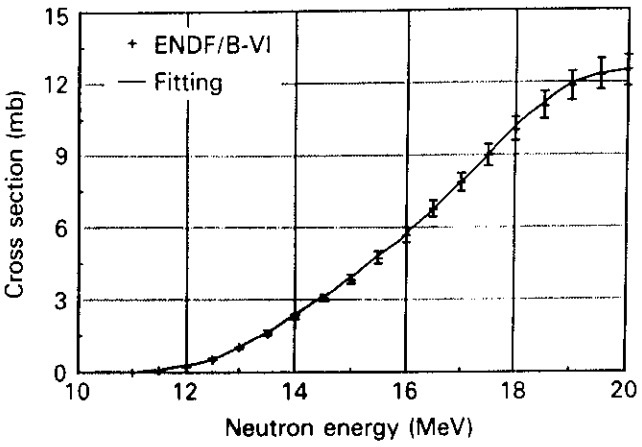

Fig. 25. Curve-fitting result for $^{184}W(n,p)$ reaction based on ENDF/B-VI data.

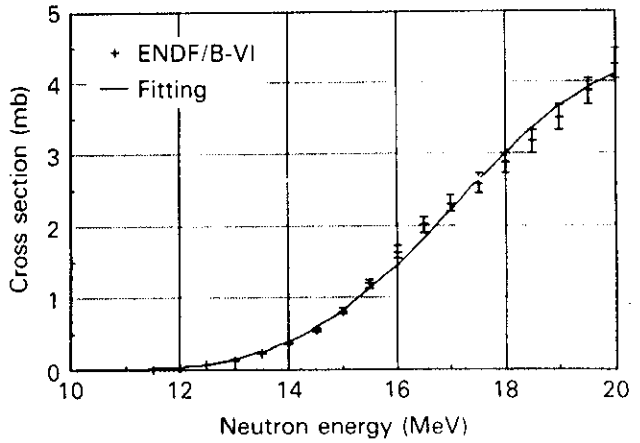

Fig. 23. Curve-fitting result for $^{186}W(n,\alpha)$ reaction based on ENDF/B-VI data.

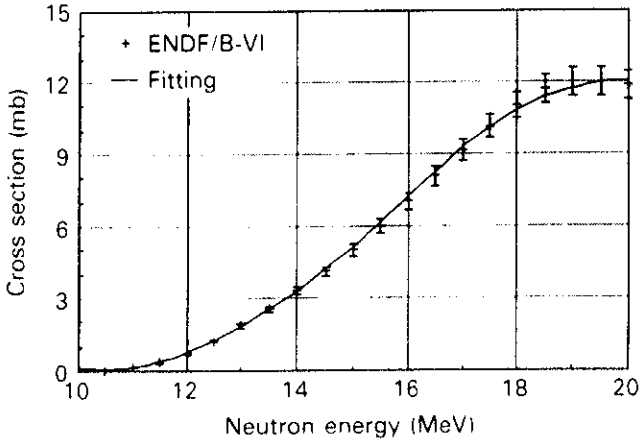

Fig. 26. Curve-fitting result for $^{183}W(n,p)$ reaction based on ENDF/B-VI data.

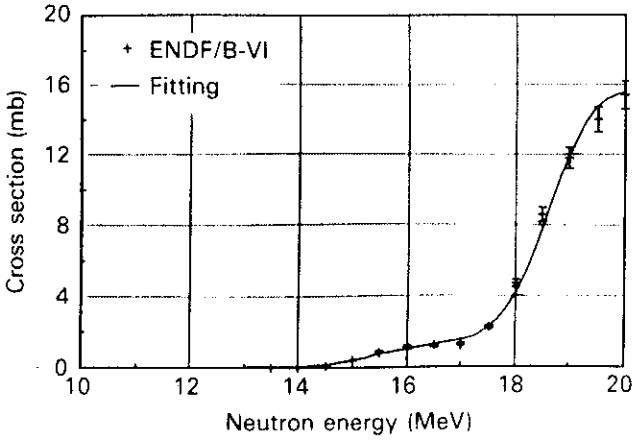

Fig. 24. Curve-fitting result for $^{186}W(n,np)$ reaction based on ENDF/B-VI data.

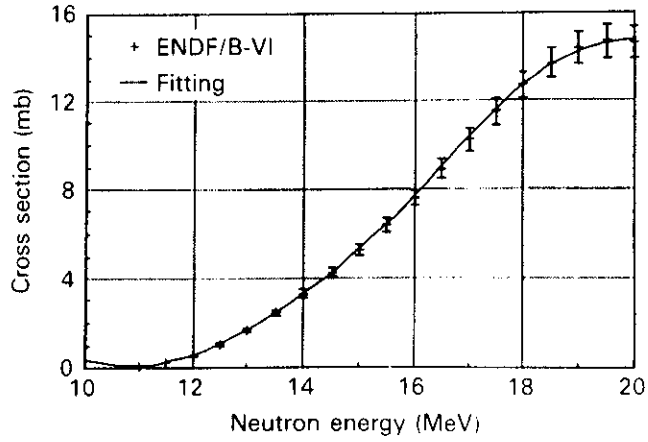

Fig. 27. Curve-fitting result for $^{182}W(n,p)$ reaction based on ENDF/B-VI data.

TABLE VI

Inputs and Results Obtained by Applying the Least-Squares Method to Eqs. (2) and (3) for Selected Reactions

Reaction	E_{th} (MeV)	$\sigma(plat.)$ (mb)	Maximum Order Taken, M	Coefficients a_m	Cutoff Energy[a] (MeV)	χ^2	Q
$^{27}Al(n,\alpha)$	3.246	250	6	a_1 = 5.577E−2[b] a_2 = −6.879E−2 a_3 = 2.528E−2 a_4 = −3.154E−3 a_5 = 1.631E−4 a_6 = −3.036E−6	6.0	6.485E−1	1.00
$^{58}Ni(n,2n)$	12.41	1220	6	a_1 = −3.421E−3 a_2 = 1.684E−2 a_3 = −5.725E−3 a_4 = 8.331E−4 a_5 = −5.560E−5 a_6 = 1.391E−6	12.2	5.575E−3	1.00
$^{90}Zr(n,2n)^{m+g}$	12.105	1250	4	a_1 = 2.083E−1 a_2 = 1.034E−1 a_3 = −1.402E−2 a_4 = 4.352E−4	12.0	2.536E−1	1.00
$^{90}Zr(n,2n)^{m}$	12.7	280	4	a_1 = −1.597E−1 a_2 = 4.423E−1 a_3 = −1.091E−1 a_4 = 9.571E−3	13.0	1.763	1.00
$^{90}Zr(n,p)^{m}$	2.206	21	3	a_1 = 1.070E−2 a_2 = −9.022E−3 a_3 = 1.929E−3	5.0	5.050	1.00
$^{90}Zr(n,\alpha)^{m}$	0.0	4.7	4	a_1 = 1.717E−1 a_2 = −5.819E−2 a_3 = 5.926E−3 a_4 = −1.567E−4	7.0	6.857	0.997
$^{91}Zr(n,p)^{m}$	1.344	23	3	a_1 = −1.680E−2 a_2 = 2.113E−3 a_3 = 5.501E−4	5.0	1.693	1.00
$^{186}W(n,p)$	3.13235	9.1	6	a_1 = −3.274 a_2 = 1.576 a_3 = −2.987E−1 a_4 = 2.784E−2 a_5 = −1.277E−3 a_6 = 2.322E−5	12.0	4.978E−1	1.00
$^{186}W(n,\alpha)$	0.0	4.5	4	a_1 = −1.527E−1 a_2 = 4.439E−2 a_3 = −4.287E−3 a_4 = 1.377E−4	11.5	8.872	0.839
$^{186}W(n,np)$	8.472	15.5	6	a_1 = −2.628 a_2 = 2.095 a_3 = −6.580E−1 a_4 = 1.017E−1 a_5 = −7.722E−3 a_6 = 2.311E−4	13.5	6.103	0.636

See footnotes at end of table.

(Continued)

TABLE VI (Continued)

Reaction	E_{th} (MeV)	$\sigma(plat.)$ (mb)	Maximum Order Taken, M	Coefficients a_m	Cutoff Energy[a] (MeV)	χ^2	Q
$^{184}W(n,p)$	2.09492	12.5	6	$a_1 = -3.010$ $a_2 = 1.413$ $a_3 = -2.609E-1$ $a_4 = 2.369E-2$ $a_5 = -1.058E-4$ $a_6 = 1.873E-5$	11.0	1.530E−1	1.00
$^{183}W(n,p)$	0.2876	12.1	5	$a_1 = 9.395E-1$ $a_2 = -2.912E-1$ $a_3 = 3.373E-2$ $a_4 = -1.760E-3$ $a_5 = 3.598E-5$	10.5	2.537	1.00
$^{182}W(n,p)$	1.034	14.8	6	$a_1 = 3.551E-1$ $a_2 = -2.555E-2$ $a_3 = -1.476E-2$ $a_4 = 2.642E-3$ $a_5 = -1.616E-4$ $a_6 = 3.504E-6$	11.0	5.042E−1	1.00

[a]Minimum energy below which Eqs. (2) and (3) do not apply.
[b]Read as 5.577×10^{-2}.

and

$$Q \equiv Q\left(\frac{\nu}{2}, \frac{\chi^2}{2}\right) = \frac{1}{\Gamma\left(\frac{\nu}{2}\right)} \int_{\nu/2}^{\infty} \exp(-t)\, t^{n/2-1}\, dt \ , \qquad (5)$$

where

Q = probability that the χ^2 should exceed a particular value by chance even for a correct model

$\nu = n - m$ = number of degrees of freedom.

This computed probability gives a quantitative measure for the goodness-of-fit of the model. If the Q value is closer to 1, the fit is better. The calculated Q and χ^2 values are presented in Table VI. As shown, all the Q values are equal to or very close to 1 except for the reaction $^{186}W(n,np)$, which has a Q value of 0.636. However, it is large enough to accept our curve fit result for this reaction.[70]

Since, in practice, activation codes require the group-structured cross sections rather than cross sections in functional form, the group cross sections were obtained by using the following formula:

$$\sigma_g = \frac{\int_g \phi\sigma(E_n)\, dE_n}{\int_g \phi\, dE_n} = \frac{\sigma(plat.) \int_g \phi\{1.0 - \exp[-f(x)]\}\, dE_n}{\int_g \phi\, dE_n} \ . \qquad (6)$$

Because we have two different neutron spectra, two sets of cross sections were obtained by using Eq. (6) in the 46-group structure of RACC (or DKRICF). The effect of these new cross sections on decay photon yield prediction will become clearer in the following sections.

VII. EFFECT OF NEW NUCLEAR DATA ON DECAY PHOTON YIELD PREDICTION

The decay data in the RACC code, particularly the decay photon spectrum and half-lives, for the nuclides of zirconium and tungsten have been rectified based on the values from the Table of Radioactive Isotopes or Table of Isotopes. Further, the reaction cross sections have been modified and implemented in the RACC cross-section library. Also, two additional RACC calculations have been carried out: one with only the modified

decay data library and another with both modified decay data and modified cross-section libraries.

VII.A. Zirconium Case

The results are depicted in Fig. 28 for each case as a function of the half-lives of the reaction products. As shown, the C/E values are clearly improved for almost every product. For ^{89}Zr, which contributes the largest amount of decay photons, the rectification of just the decay data alone constitutes a large improvement in the first and third cases, whereas the second case has the best results when both decay and cross-section data are modified. However, these results are all acceptable since they lie within the experimental error. Experimental error for ^{89}Zr decay photon yield is ~2 to 3%. The fact that the computed decay rates are consistently underestimated for all products in all cases even with the corrected data necessitates further investigation of the experimental results.

VII.B. Tungsten Case

Figure 29 summarizes the results of tungsten for the two different irradiation cases considered in this study. Again, a great improvement in the computed values is clearly observed for virtually every product in both cases. The improvements in calculated values for ^{186}Ta, ^{185}Ta, ^{184}Ta, ^{183}Ta, and ^{183}Hf are particularly significant. For ^{187}W, which is the largest contributor, the polynomial approach to improving the excitation function could not be applied because of the complexity of the excitation function for the ^{186}W(n,γ) reaction, which is a nonthreshold reaction in the first place. Instead, the reaction cross section given in ENDF/B-VI was adopted, and there is no improvement in the C/E value for ^{187}W. The exact sources of the overestimation of the computed decay photon yield from ^{187}W cannot be ascertained at this stage. But, the lower part of the neutron energy spectrum, where most of the (n,γ) reaction originates, has too few neutrons to be considered statistically reliable for an MCNP simulation, and there is some difficulty in the modeling of all the geometrical and material details. Of course, the statistical error of the lower energy neutrons does not solely explain the large overestimation of the decay photons from ^{187}W. Other factors, such as the influence of the neutron self-shielding on the experimental data, should also be considered. Further study is recommended.

VIII. APPLICATION OF THE NEW NUCLEAR DATA TO THE ITER DESIGN

Finally, several activation analyses of the proposed ITER design were performed to gain some insight into the effect of our modified and corrected data on a real application problem. The reference ITER outboard design in the technology phase,[71] where the tungsten is used as a 0.05-cm coating on the first-wall system, is schematically depicted in Fig. 30. Two Li_2ZrO_3 breeder zones, each 0.8 cm thick, are used in this design. Because the study specifically concerns the tungsten coating and the breeder zones, some arbitrarily chosen thickness of stainless steel was placed beyond the blanket zone in order to simulate the contribution of backscattered neutrons into the blanket. However, the contribution of these neutrons to activation of the tungsten and the breeding zones appears to be insignificant. A set of three different calculations was performed:

1. reference case: 0.05-cm tungsten first-wall coating, two 0.8-cm Li_2ZrO_3 zones, and a 30-cm stainless steel shield
2. Li_2SiO_3 as a breeder instead of Li_2ZrO_3 to compare the activation characteristics due to zirconium with those of silicon where the new zirconium data can be used
3. tungsten as a shield (same as case 1 except that the 30-cm stainless steel zone is broken into 15 cm of stainless steel and 15 cm of tungsten).

Note that the last case is included just to see the effect of a softer neutron energy spectrum on the activation levels due to tungsten when the new data are used. In all the neutronics calculations, transport and activation, cylindrical modeling was used by taking the center of the plasma as the axis of a cylinder. One should refer to Ref. 33 for a more complete activation analysis of the real ITER design, including the inboard and outboard and the physics and technology phases.

VIII.A. Transport Calculation

A one-dimensional neutron transport code, ANISN (Ref. 72), was used to determine the neutron distribution along each zone shown in Fig. 30. The ANISN calculation used a coupled 30 neutron, 12 gamma group structure for the cross section that was derived from ENDF/B-V, and it used P_3S_8 approximation. Then, since the RACC calculation requires a 46-group structure for the neutron flux input, the 30-group flux from ANISN was expanded into 46 groups by requiring that the total number of neutrons be conserved. The numerical error produced in this process is expected to be small.

VIII.B. Activation Calculation

Specific photon yields (number of photons per cubic centimetre) in each tungsten and breeding zone as a function of both before- and after-shutdown times were computed by using RACC along with an appropriate flux input. During the RACC calculation, different combinations of the decay and cross-section data libraries were used to deduce the separate effects of the decay and cross-section data on the predicted photon

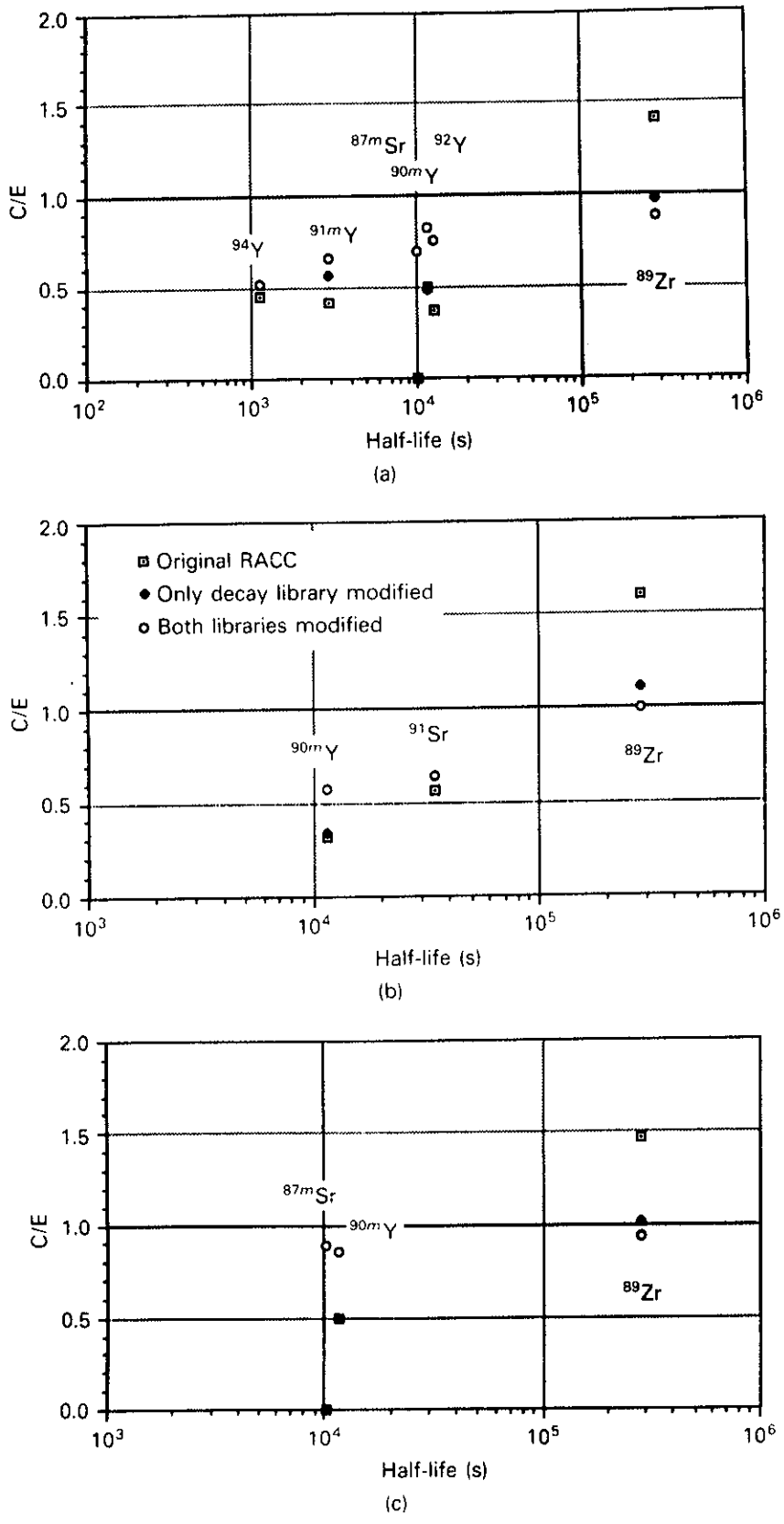

Fig. 28. Effect of improved decay data and cross-section data on the decay rate C/E ratios for the zirconium sample subjected to the 10-cm spectrum for (a) T_r = 30 min and T_c = 56.5 min; (b) T_r = 9 h and T_c = 17 h, 15.7 min and to the 82-cm spectrum for (c) T_r = 10 h and T_c = 3 h, 13.5 min.

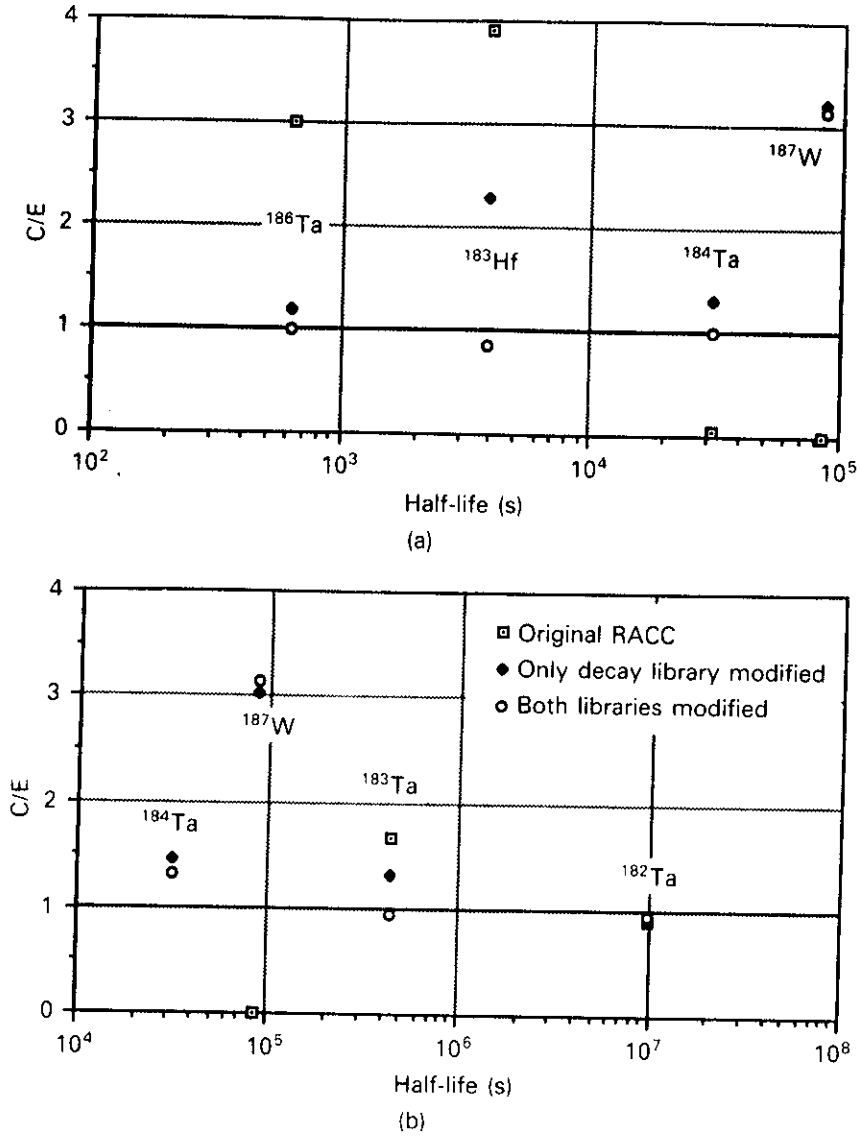

Fig. 29. Effect of improved decay data and cross-section data on the decay rate C/E ratios for the tungsten sample subjected to the 10-cm spectrum: (a) T_r = 30 min and T_c = 37.3 min and (b) T_r = 9 h and T_c = 2 days, 19 h, 3.5 min.

yields. Those combinations are (a) original decay data library + original cross-section library, (b) modified decay data library + original cross-section library, and (c) both modified decay data and cross-section libraries. Other important input parameters employed are 1 MW/m^2 of neutron wall loading and 1 yr of continuous operation time. Note, however, that in the real ITER device, the neutron wall loading and operation time will be different depending on inboard and outboard, physics or technology phase, etc. (Ref. 33).

VIII.B.1. Case 1

Figures 31 and 32 show the specific photon yield in the tungsten coating zone as a function of the before- and after-shutdown times, respectively. Included in the figures are ratios of the photon yield obtained when both modified decay and cross-section libraries are used to that obtained when original RACC libraries are used. The figures indicate that the original RACC libraries, because of the inadequacy of the decay data library, underestimate the photon yield by as much as a factor of 1000 in the tungsten zone regardless of the before- and after-shutdown times. The difference mainly originates from the wrong decay data assignment of ^{187}W as cited earlier. However, the degree of underestimation decreases as after-shutdown time increases, and it finally becomes negligible 1 month after shutdown. This is because we have corrected only data pertinent to isotopes with relatively shorter half-lives. The longest one

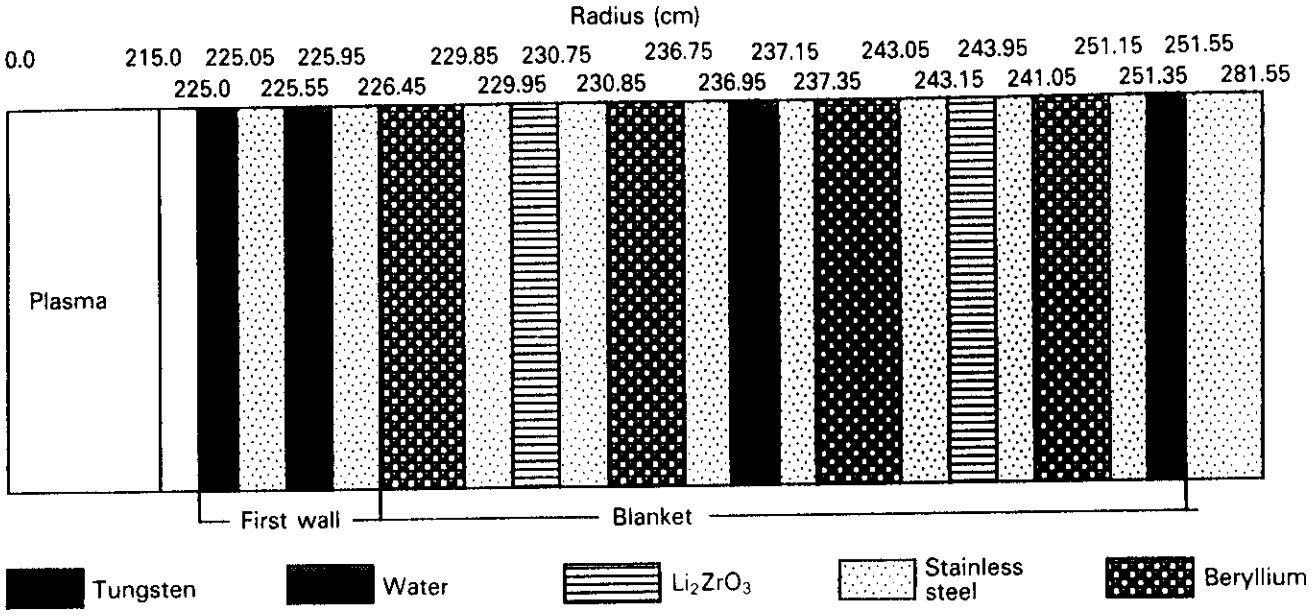

Fig. 30. Geometry and material composition of proposed ITER outboard design.

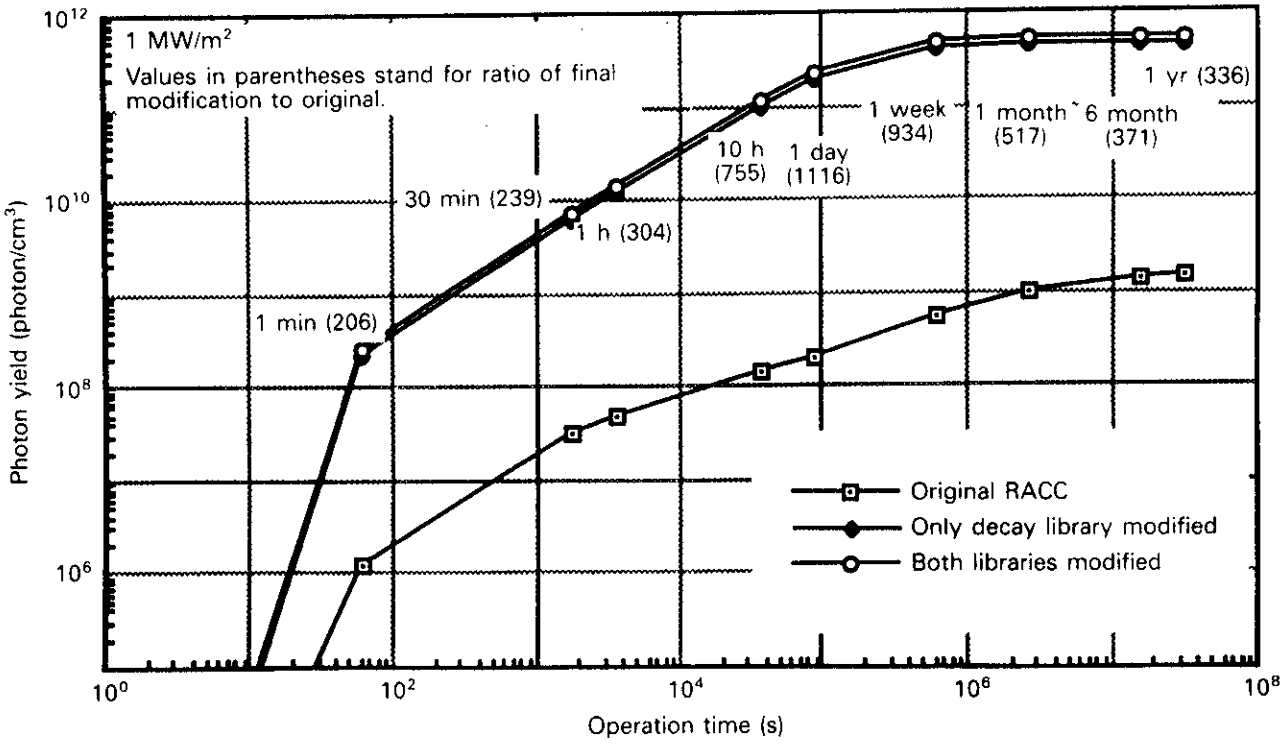

Fig. 31. Specific photon yield in the tungsten coating zone as a function of operation time calculated by using the three different data libraries in RACC.

involved in our study was ^{182}Ta (~115.0 days), but its contribution is very small.

Figures 33 and 34 display the specific photon yield in the Li_2ZrO_3 breeding zone as a function of the before- and after-shutdown times, respectively. As opposed to the tungsten zone, the differences caused by using different libraries are very small, but the original RACC libraries tend to overestimate the photon

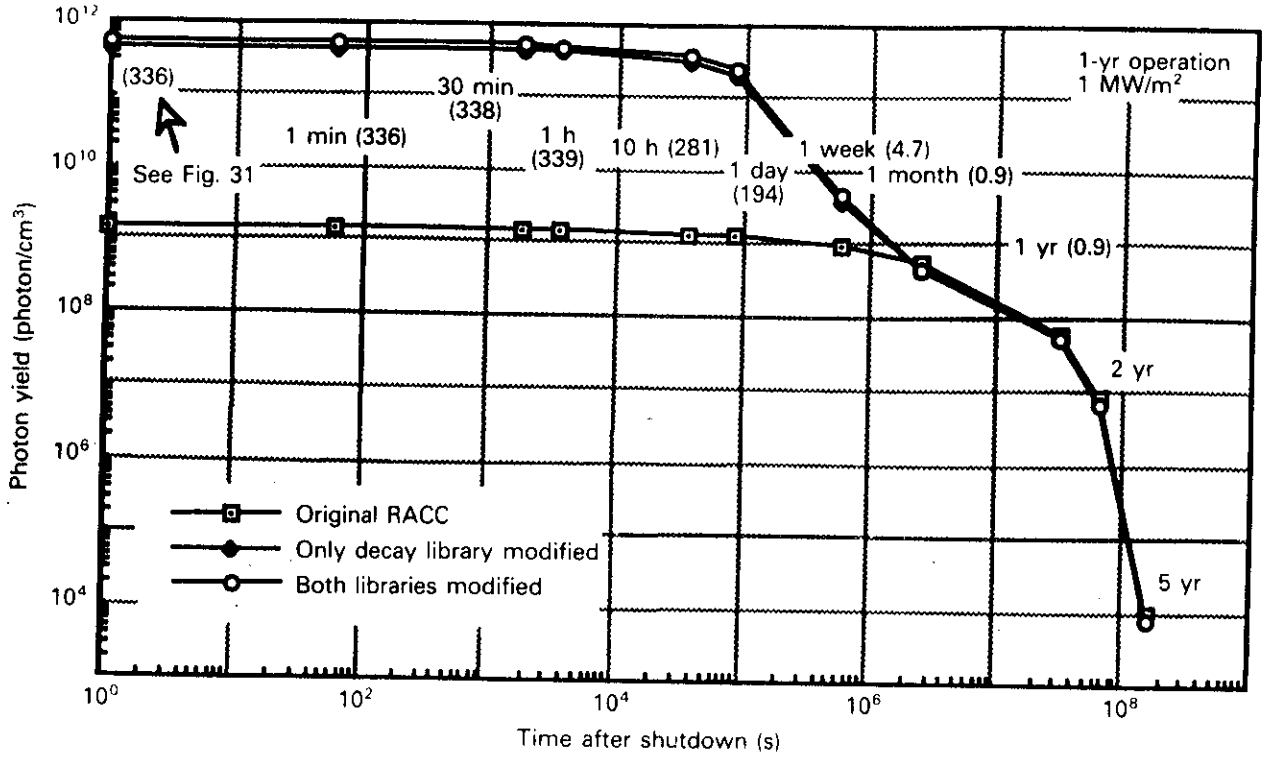

Fig. 32. Specific photon yield in the tungsten coating zone as a function of time after shutdown calculated by using the three different data libraries in RACC.

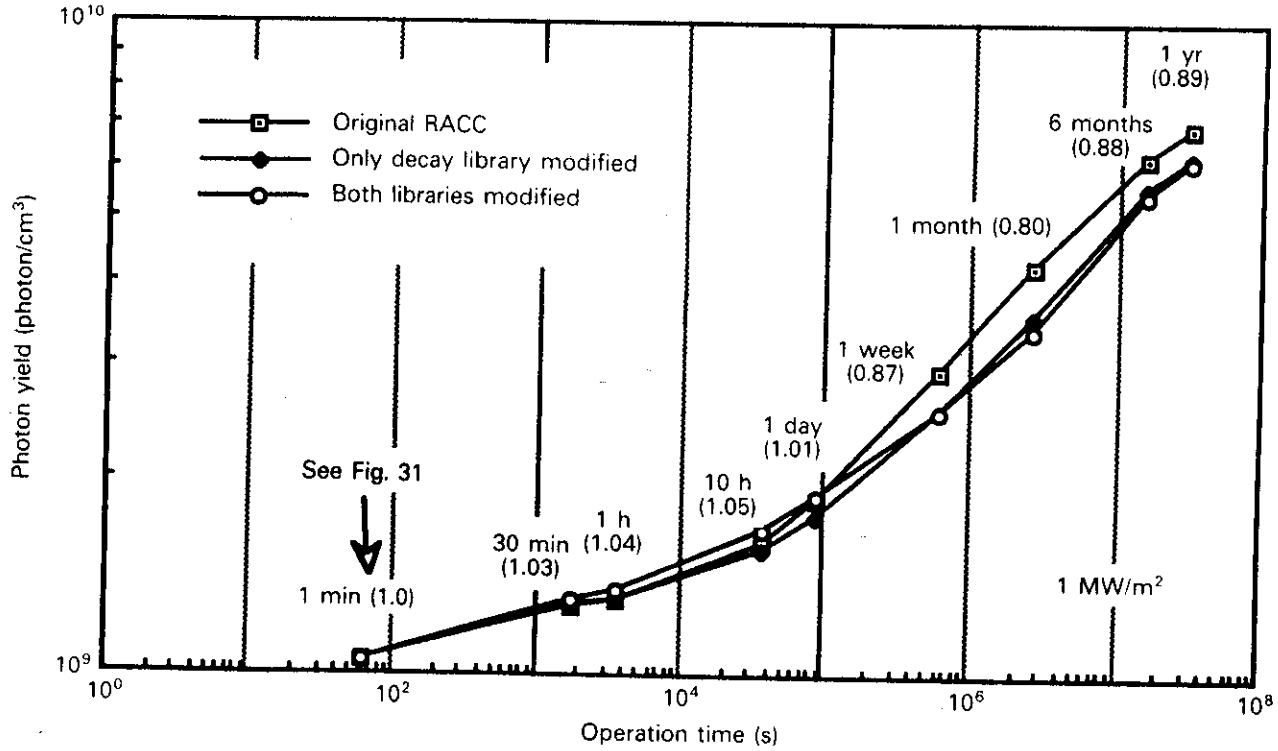

Fig. 33. Specific photon yield in the Li_2ZrO_3 zone as a function of operation time calculated by using the three different data libraries in RACC.

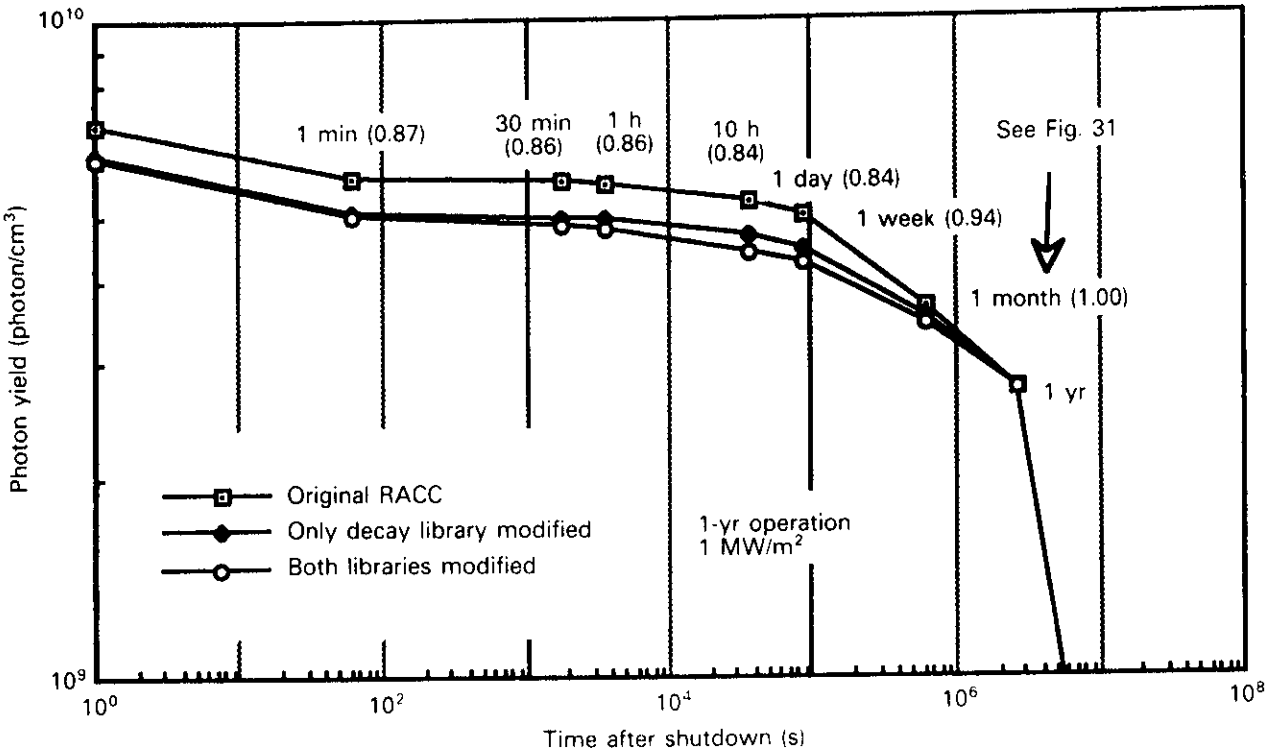

Fig. 34. Specific photon yield in the Li_2ZrO_3 zone as a function of time after shutdown calculated by using the three different data libraries in RACC.

yield by ~10 to 15%. However, these differences decrease as the after-shutdown times increase, until ~1 month after shutdown. After that, ^{95}Zr [$T_{1/2}$ = ~45 days, $^{96}Zr(n,2n)$], whose data were not investigated in this study, turns out to be the leading photon emitter.

VIII.B.2. Case 2

Figures 35 and 36 show the results of the comparison study of the specific decay photon yields due to Li_2ZrO_3 and Li_2SiO_3 as a function of before- and after-shutdown times, respectively. As shown in Fig. 35, the decay photon yield from Li_2SiO_3 becomes saturated faster than that of Li_2ZrO_3, and it emits about two orders of magnitude more photons during the operation. However, after shutdown, the decay photon yield from Li_2SiO_3 dies away very quickly (Fig. 36), during an ~1-h span. These phenomena are due to the short-half-life reaction product ^{28}Al [2.24 min, $^{28}Si(n,p)^{28}Al$], which is the dominant contributor to the short-term decay photons whenever silicon exists in the fusion-neutron field. This behavior is seen regardless of whether the new data for zirconium are used or not. However, we should use caution in saying that Li_2SiO_3 is better than Li_2ZrO_3 from the radiological point of view, because the nuclear data pertinent to silicon were not checked in this study. A more refined study is required to investigate the nuclear data of silicon before any conclusion can be stated.

VIII.B.3. Case 3

Figures 37 and 38 display the specific decay photon yield in the 15-cm tungsten shield zone as a function of before- and after-shutdown times, respectively. Note that the 15-cm stainless steel zone is placed in front of the tungsten zone to make the neutron energy spectrum softer so as to see the effect of the softer spectrum on the characteristics of the decay photon yield for tungsten. The functional behavior of both the before- and after-shutdown photon yields is very similar to that in the tungsten coating zone (Figs. 31 and 32), where the neutron spectrum is harder. However, the ratios of the final values, which were obtained after all the pertinent nuclear data were corrected, to the original values are rather different in each case. In general, the ratios are larger in this case than in case 1 because $^{186}W(n,\gamma)^{187}W$, which is the dominant reaction channel in terms of the decay photon emission as discussed before, becomes more important in the softer neutron spectrum. The ratios in this case are ~1.2 to 1.6 times larger than those in case 1. Even though the results

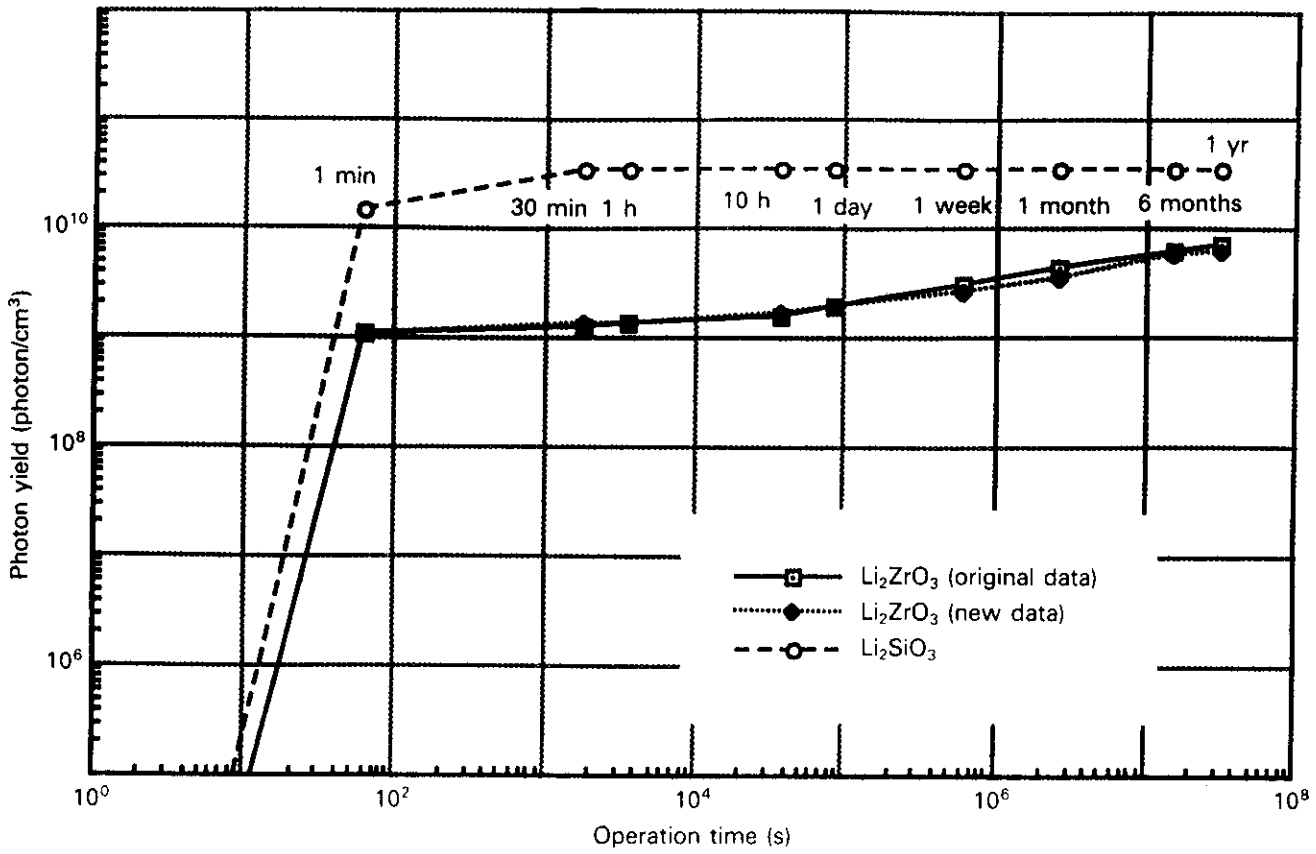

Fig. 35. Comparison of the specific decay photon yields in Li_2ZrO_3 as a function of operation time.

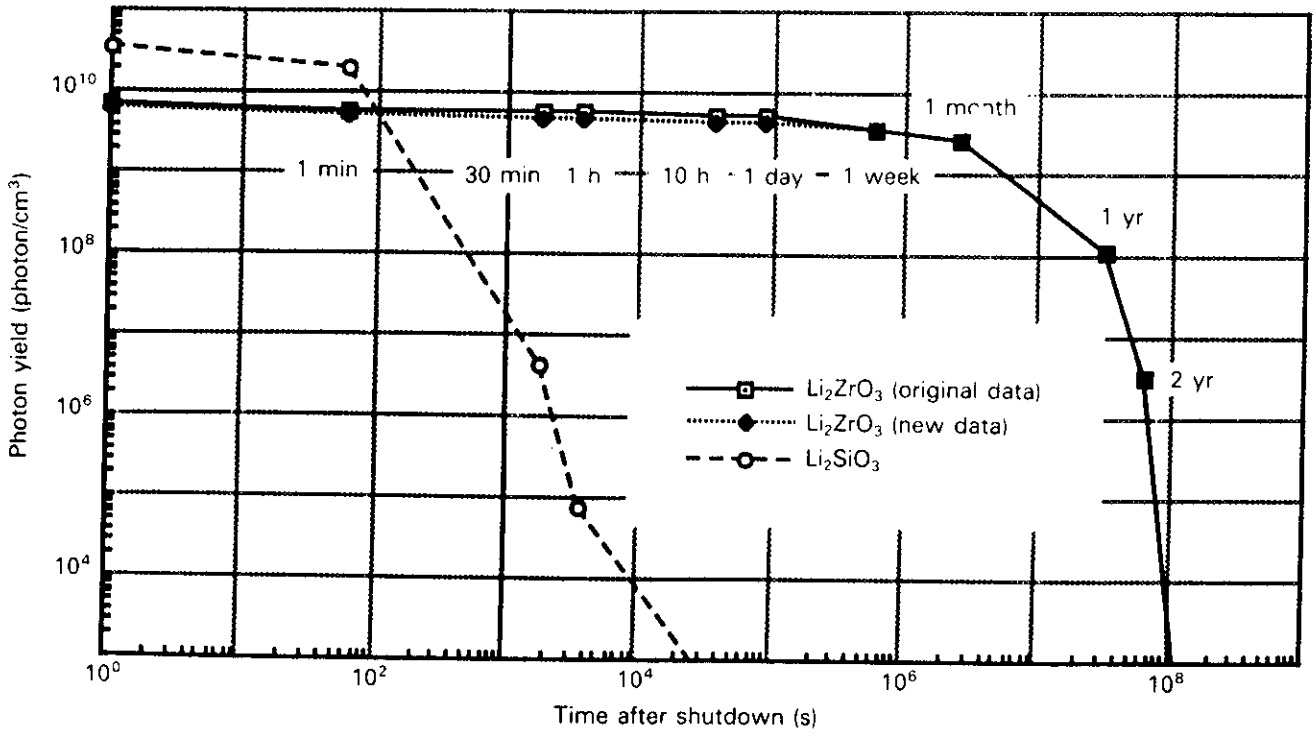

Fig. 36. Comparison of the specific decay photon yields in Li_2ZrO_3 as a function of time after shutdown.

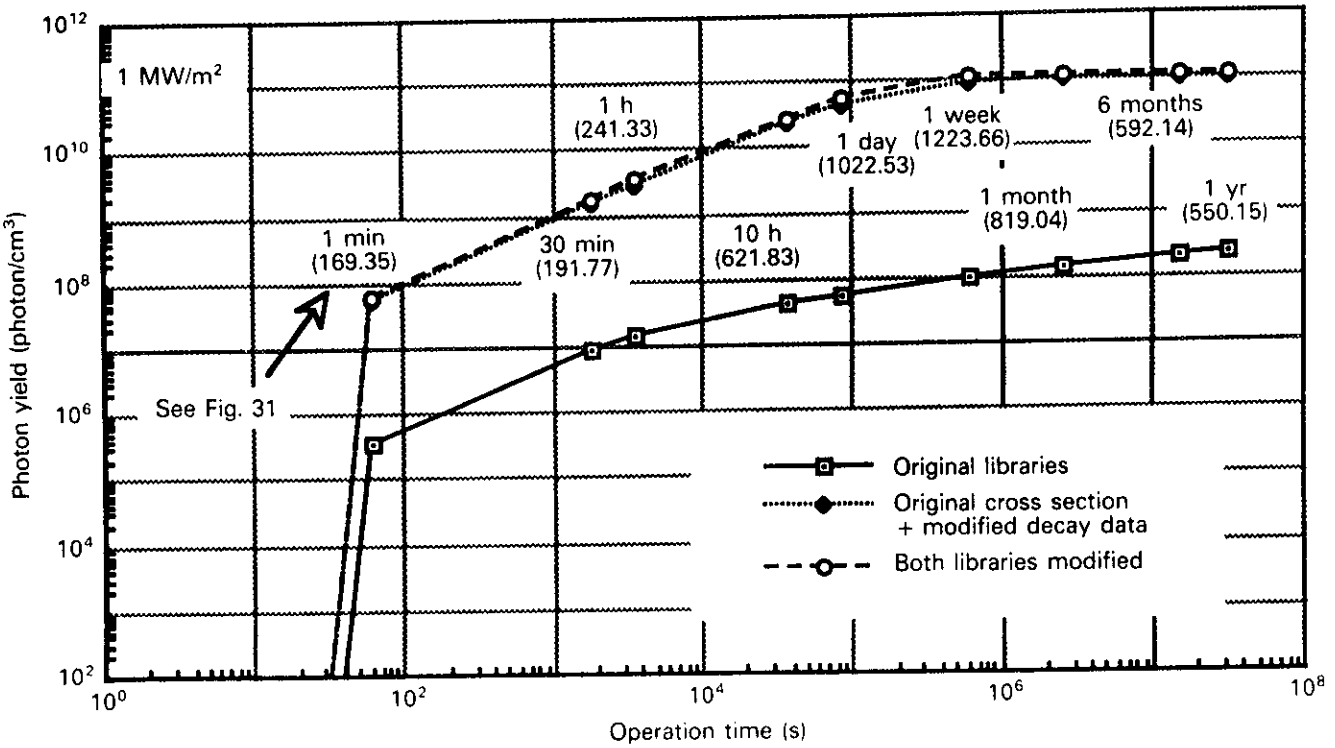

Fig. 37. Specific photon yield in 15-cm-thick tungsten shield zone as a function of operation time (a 15-cm-thick stainless steel zone is placed in front of the tungsten zone).

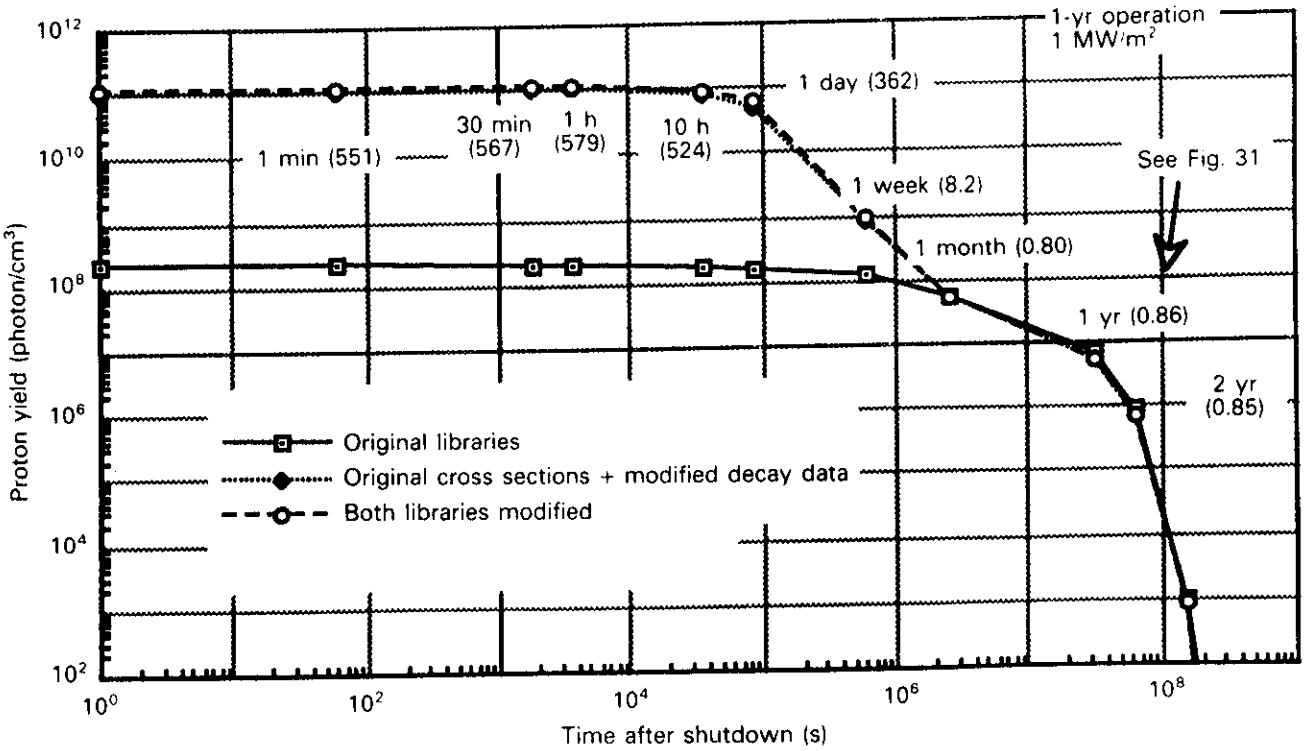

Fig. 38. Specific photon yield in 15-cm-thick tungsten shield zone as a function of time after shutdown (a 15-cm-thick stainless steel zone is placed in front of the tungsten zone).

given here could be expected prior to the analysis, this confirms that our correction of the nuclear data is in the right direction.

IX. SUMMARY AND CONCLUSIONS

Measured decay rates resulting from neutron irradiation of zirconium and tungsten samples in a typical fusion environment have been compared with the results of calculations by four representative codes widely used in the fusion community: REAC*2, DKRICF, RACC, and ACT4. The main objective of the comparison study was to check the validity of the mathematical models of the codes themselves as well as of the associated nuclear data—decay data and transmutation cross sections—relevant to zirconium and tungsten. Direct intercomparison of different mathematical models used in various codes, which was possible when all pertinent input data were kept the same, showed that the large discrepancies between the codes do not originate from the different mathematical models; rather, they come from differences in the nuclear data.

The analysis of the computed decay rates based on the measured values identified that the following reactions and their products [$^{90}Zr(n,2n)^{89m,g}Zr$, $^{90}Zr(n,p)$-^{90m}Y, $^{90}Zr(n,\alpha)^{87m}Sr$, and $^{91}Zr(n,p)^{91m}Y$ for the zirconium case and $^{186}W(n,\gamma)^{187}W$, $^{186}W(n,p)^{186}Ta$, $^{186}W(n,np)(n,d)^{185}Ta$, $^{184}W(n,p)^{184}Ta$, $^{183}W(n,p)$-^{183}Ta, $^{182}W(n,p)^{182}Ta$, and $^{186}W(n,\alpha)^{183}Hf$ for the tungsten case] are most important in terms of emitting decay photons, but their associated decay data and cross sections are not adequate. The decay data were rectified on the basis of the Table of Radioactive Isotopes, and the cross sections were improved by a simple curve-fitting procedure based on the ACTL formulation. A new fitting method, which treats mainly the threshold reactions, was designed to take full advantage of our wealth of experimental data over a wide energy range and was made inherently to follow the experimental trend of the excitation function. The modified and improved decay data and cross sections were implemented in RACC, which was selected as a representative code in a second series of calculations, and the computation was performed again. A great improvement in the computed results was observed for both sample cases except for in the $^{186}W(n,\gamma)^{187}W$ reaction since the improvement of (n,γ) reactions was not considered in this study.

The expansion of our work to other materials such as iron, nickel, cobalt, copper, and stainless steel is recommended. Finally, our modified and corrected decay and cross-section data were applied to the ITER outboard design. In ITER, tungsten is a candidate first-wall coating material, and Li_2ZrO_3 can be used as a breeding material. Specific photon yields in each zone were computed as a function of both the before- and after-shutdown times. An increase by as much as three orders of magnitude in the photon yield in the tungsten zone and an ~10 to 15% reduction in photon yield in the breeding zone were observed when the corrected data were used.

Even though this work dealt exclusively with zirconium and tungsten, previous analysis[44-51] had already pointed out many discrepancies related to decay data and activation cross sections for other materials. Therefore, it is necessary to review the decay and cross-section data for all isotopes included in the data libraries of all radioactivity codes. It is recommended that the decay data library should be reviewed first because the decay data are relatively easy to correct and they have great significance in real applications. Improvement of the cross sections is more difficult, but the new curve-fitting method developed in this paper can be very helpful, at least for the threshold reactions, if there are good experimental data over a wide range of energy.

ACKNOWLEDGMENTS

This work was supported by DOE. The experimental data on radioactivity were obtained at the Fusion Neutron Source facility at JAERI as part of the U.S.-JAERI collaborative program on fusion neutronics. Y. Ikeda (JAERI) and A. Kumar (University of California, Los Angeles) led the experimental activity on radioactivity measurements.

REFERENCES

1. D. STEINER and A. P. FRAAS, "Preliminary Observations on the Radiological Implications of Fusion Power," *Nucl. Saf.*, **13**, 353 (1972).

2. W. F. VOGELSANG et al., "Transmutations, Radioactivity, and Afterheat in a Deuterium-Tritium Tokamak Fusion Reactor," *Nucl. Technol.*, **22**, 379 (1974).

3. R. W. CONN, T. Y. SUNG, and M. A. ABDOU, "Comparative Study of Radioactivity and Afterheat in Several Fusion Reactor Blanket Designs," *Nucl. Technol.*, **26**, 391 (1975).

4. R. W. CONN, K. OKULA, and A. W. JOHNSON, "Minimizing Radioactivity and Other Features of Elemental and Isotopic Tailoring of Materials for Fusion Reactors," *Nucl. Technol.*, **41**, 389 (1978).

5. M. YOUSSEF and R. W. CONN, "Induced Radioactivity and Influence of Materials Selection in Deuterium-Deuterium and Deuterium-Tritium Fusion Reactors," *Nucl. Technol.*, **3**, 361 (1983).

6. M. C. STAUBER, "Preface: Radioactivity of Fusion Structures," *Nucl. Technol./Fusion*, **4**, 525 (1983).

7. G. R. HOPKINS and E. T. CHENG, "Low Activation Fusion Rationale," *Nucl. Technol./Fusion*, **4**, 528 (1983).

8. E. T. CHENG, "Radioactivation Characteristics for Deuterium-Tritium Fusion Reactors," *Nucl. Technol./Fusion*, **4**, 545 (1983).

9. J. JUNG, "An Analysis of Activation and the Impact of Tritium Breeding Media and Structural Materials for a Commercial Tokamak Fusion Reactor Design," *Nucl. Technol./Fusion*, **4**, 566 (1983).

10. L. KU and J. G. KOLIBAL, "Radioactivation Characteristics for the Tokamak Fusion Test Reactor," *Nucl. Technol./Fusion*, **4**, 586 (1983).

11. E. T. CHENG and G. R. HOPKINS, "The Nuclear Design of a Very Low Activation Fusion Reactor," GA-A17012, GA Technologies (1983).

12. G. R. HOPKINS et al., "Low Activation Fusion Reactor Design Studies," GA-A17018, GA Technologies (1983).

13. G. P. LASCHE and J. A. BLINK, "The Dependence of Neutron Induced Radioactivity in Fusion Reactors on Geometric Design Parameters," *Nucl. Technol. Fusion*, **4**, 823 (1983).

14. J. R. POWELL and J. A. FILLO, "Prospects for Low-Activity Aluminum Structures," *Nucl. Technol. Fusion*, **4**, 561 (1983).

15. R. W. CONN et al., "Lower Activation Materials and Magnetic Fusion Reactors," *Nucl. Technol. Fusion*, **5**, 291 (1984).

16. E. E. BLOOM et al., "Low Activation Materials for Fusion Applications," *J. Nucl. Mater.*, **122 & 123**, 17 (1984).

17. F. M. MANN, "Reduced Activation Calculations for the Starfire First Wall," *Fusion Technol.*, **6**, 273 (1984).

18. G. LOGAN, "A Rationale for Fusion Economics Based in Inherent Safety," *J. Fusion Energy*, **4**, 245 (1985).

19. H. FUKUMOTO, "New Approach to Neutron-Induced Transmutation, Radioactivity and Afterheat Calculations and Its Application to Fusion Reactors," *J. Nucl. Sci. Technol.*, **23**, 97 (1986).

20. K. OISHI et al., "Experiment and Analysis of Induced Activities in Concrete Irradiated by 14-MeV Neutrons," *Fusion Technol.*, **10**, 579 (1986).

21. S. FETTER, E. T. CHENG, and F. M. MANN, "Long-Term Radioactivity in Fusion Reactors," *Fusion Eng. Des.*, **6**, 123 (1988).

22. T. NODA et al., "Materials Selection for Reduced Activation of Fusion Reactors," *J. Nucl. Mater.*, **155-157**, 581 (1988).

23. L. R. GREENWOOD and D. L. BOWERS, "Production of Long-Lived Activities in Fusion Materials," *J. Nucl. Mater.*, **155-157**, 585 (1988).

24. J. SANZ et al., "Impact of the Neutron Flux on Transmutation Products at Fusion Reactor First-Walls," *J. Nucl. Mater.*, **155-157**, 592 (1988).

25. H. ATTAYA et al., "Activation Characteristics of Different Steel Alloys Proposed for Near Term Fusion Reactors," *Fusion Technol.*, **15**, 893 (1989).

26. H. Y. KHATER et al., "Activation Analysis for the Aqueous Self-Cooled Blanket and Shield of ITER," *Fusion Technol.*, **15**, 900 (1989).

27. E. T. CHENG, "Radioactivity Aspects of Fusion Reactors," *Fusion Eng. Des.*, **8-10** (1989).

28. M. ZUCCHETTI, "Impurity Concentration Limits and Activation in Fusion Reactor Structural Materials," *Fusion Technol.*, **19**, 294 (1991).

29. C. P. C. WONG et al., "ARIES-I SiC Composite Activation Blanket Design," *Fusion Technol.*, **19**, 938 (1991).

30. J. S. HERRING et al., "Activation Product Safety in the ARIES-I Reactor Design," *Fusion Technol.*, **19**, 1386 (1991).

31. T. J. DORAN and G. R. LONGHURST, "Safety and Environmental Aspects of HYLIFE-II," *Fusion Technol.*, **19**, 1392 (1991).

32. Y. SEKI et al., "Activation Products Effluents Evaluation for ITER," *Fusion Technol.*, **19**, 1831 (1991).

33. H. ATTAYA et al., "US-ITER Activation Analysis," *Fusion Technol.*, **19**, 1837 (1991).

34. K. OISHI et al., "Measurement and Analysis of Induced Activities in Concrete Components Irradiated by 14-MeV Neutrons," *Fusion Technol.*, **18**, 291 (1990).

35. H. Y. KHATER et al.,"Environmental and Safety Aspects of ORISIS: A Heavy Ion Beam Driven IFE Reactor," *Fusion Technol.*, **21**, 2138 (1992).

36. M. YOUSSEF and R. W. CONN, "On Isotopic Tailoring for Fusion Reactor Radioactivity Reduction," *Fusion Technol.*, **4**, 1177 (1983).

37. E. T. CHENG, "Nuclear Data Requirements for Fusion Reactor Transport Calculations and Testing of ENDF/B-V and VI Libraries," *Nuclear Data for Fusion Reactor Technology*, IAEA-TECDOC-457, International Atomic Energy Agency (1986).

38. E. T. CHENG et al. "International Fusion Activation Calculation Comparison Study," TSIR-12, TSI Research Inc. (1991).

39. "First Results of FENDL-1 Testing and Start of FENDL-2," *Summary Report Consultants' Mtg.*, Vienna,

Austria, June 25-28, 1990, INDC(NDS)-241, International Atomic Energy Agency (Nov. 1990).

40. F. M. MANN, "REAC*2: User's Manual and Code Description," WHC-EP-0282, Westinghouse Hanford Company (1989).

41. D. L. HENDERSON and O. YASAR, "DKRICF: A Radioactivity and Dose Rate Calculation Code Package," UWFDM-714, University of Wisconsin (1986).

42. J. JUNG, "Theory and Use of the Radioactivity Code RACC," ANL/FPP/TM-122, Argonne National Laboratory (1979).

43. Y. SEKI et al., "THIDA-2: An Advanced Code System for Calculation of Transmutation, Activation, Decay Heat and Dose Rate," JAERI-1301, Japan Atomic Energy Research Institute (1986).

44. A. KUMAR, M. ABDOU, Y. IKEDA, and C. KONNO, "Radioactivity and Nuclear Heating Measurements for Fusion Application," *Fusion Technology, 1990*, p. 872, B. E. KEEN et al., Eds., Elsevier Science Publishers (1991).

45. A. KUMAR et al., "Experiments and Analysis for Measurements of Decay Heat Related Induced Activities in Simulated Line Source Driven D-T Neutron Fields of Phase IIIA: USDOE/JAERI Collaborative Program on Fusion Neutronics," *Fusion Technol.*, **19**, 1859 (1991).

46. A. KUMAR et al., "Analysis of Induced Activities Measurements Related to Decay Heat in Phase IIC Experimental Assembly: USDOE/JAERI Collaborative Program on Fusion Neutronics," *Fusion Technol.*, **19**, 1909 (1991).

47. Y. IKEDA et al., "Experiment on Induced Activities and Decay Heat in Simulated D-T Neutron Field: USDOE JAERI Collaborative Program on Fusion Neutronics," *Fusion Technol.*, **19**, 1961 (1991).

48. Y. IKEDA et al., "Experimental Verification of the Current Data and Methods for Induced Radioactivity and Decay Heat Calculations in D-T Fusion Reactors," presented at 2nd Int. Symp. Fusion Nuclear Technology, Karlsruhe, Germany, June 2-7, 1991.

49. A. KUMAR, "Foreign Trip Reports, for Period November 23-December 17, 1988 and May 22-June 23, 1989, on Experiment on Radioactivity and Nuclear Heat Deposition Rates Measurements," University of California-Los Angeles (1989).

50. A. KUMAR et al., "Radioactivity and Decay Heat Integral Measurements in Simulated Fusion Environment," presented at U.S.-Japan Workshop on Fusion Neutronics, Osaka, Japan, May 24-25, 1989.

51. A. KUMAR, "Measurement and Analysis of Decay Radioactivity Data on Tungsten," Memo, University of California-Los Angeles (Feb. 1991).

52. E. BRIESMEISTER, "MCNP – A General Monte Carlo Code for Neutron and Photon Transport," LA-7396-M, Rev. 2, Los Alamos National Laboratory (1986).

53. "ENDF-102: Data Format and Procedures for the Evaluated Nuclear Data File ENDF/B-VI," BNL-NCS-44945, Brookhaven National Laboratory (1990).

54. E. BROWNE et al., *Table of Radioactive Isotopes*, John Wiley & Sons, New York (1986).

55. C. M. LEDERER et al., *Table of Isotopes*, 6th and 7th eds., John Wiley & Sons, New York (1967 and 1978).

56. R. R. KINSEY, "Evaluated Neutron Data File, ENDF/B-V," ENDF Summary Documentation, ENDF-201, 3rd ed., Brookhaven National Laboratory (1979).

57. N. GARDNER and R. J. HOWERTON, "ACTL: Evaluated Neutron Activation Cross Section Library -Evaluation Technique and Reaction Index," UCRL-50400, Vol. 18, Lawrence Livermore National Laboratory (1978).

58. J. P. BUTLER and D. C. SANTRY, "Excitation Curves for the Reactions $Al^{27}(n,\alpha)$ and $Mg^{24}(n,p)Na^{24}$," *Can. J. Phys.*, **41**, 472 (1963).

59. H. LISKIEN and A. PAULSEN, "Cross Sections for the $Cu^{63}(n,\alpha)Co^{60}$, $Ni^{60}(n,p)Co^{60}$ and Some Other Threshold Reactions Using Neutrons from the $Be^{9}(\alpha,n)C^{12}$ Reaction," *Nukleonik*, **8**, 315 (1966).

60. A. PAULSEN and H. LISKIEN, "Cross Sections for the Reactions $Mn^{55}(n,2n)$, $Co^{59}(n,2n)$, $Mg^{24}(n,p)$ and $Al^{27}(n,\alpha)$ in the 12.6-19.6 MeV Energy Region," *J. Nucl. Energy*, **19**, 907 (1965).

61. Y. IKEDA et al., "Activation Cross Section Measurements for Fusion Reactor Structural Materials at Neutron Energy from 13.3 to 15.0 Mev Using FNS Facility," JAERI-1312, Japan Atomic Energy Research Institute (1988).

62. A. PAVLIK et al., "Neutron-Induced Reactions on Ni-58," *J. Nucl. Sci. Eng.*, **90**, 186 (1985).

63. D. R. NETHAWAY, "Cross Sections for Several $(n,2n)$ Reactions at 14 MeV," *Nucl. Phys. A*, **190**, 635 (1972).

64. R. J. PRESTWOOD and B. P. BAYHURST, "$(n,2n)$ Excitation Functions of Several Nuclei from 12.0 to 19.8 MeV," *Phys. Rev.*, **121**, 1438 (1961).

65. B. P. BAYHURST et al., "Cross Sections for $(n,2n)$ Reactions Between 7.5 and 28 MeV," *Phys. Rev. C*, **12**, 451 (1975).

66. Y. KANDA, "The Excitation Functions and Isomeric Ratios for Neutron Induced Reactions on Mo-92 and Zr-90," *Nucl. Phys. C*, **185**, 177 (1972).

67. A. ABBOUD et al., "Isomeric Cross Section Ratios and Total Cross Sections for the $^{74}Se(n,2n)^{73g,m}Se$,

$^{90}Zr(n,2n)^{89m,g}Zr$, and $^{92}Mo(n,2n)^{91g,m}Mo$ Reactions," *Nucl. Phys. A*, **139**, 42 (1969).

68. M. MAJAH and S. M. QAIM, "Activation Cross Sections of Neutron Threshold Reactions on Some Zirconium Isotopes in the 5.4 to 14.6 MeV Energy Range," *J. Nucl. Sci. Eng.*, **104**, 271 (1990).

69. A. MARCINKOWSKI et al., "Cross Sections of the (n,p) Reaction on Zirconium Isotopes," *Nucl. Phys. A*, **510**, 93 (1990).

70. W. H. PRESS et al., *Numerical Recipes*, 2nd ed., p. 614, Cambridge University Press (1992).

71. Y. GOHAR et al., "U.S. Solid Breeder Blanket Design for ITER," *Fusion Technol.*, **19**, 1538 (1991).

72. W. W. ENGLE, Jr., "User's Manual for ANISN, A One-Dimensional Discrete Ordinates Transport Code with Anisotropic Scattering," K-1693, Oak Ridge Gaseous Diffusion Plant (1967).